



HAL
open science

Identification of distinct pathological signatures induced by patient-derived α -synuclein structures in nonhuman primates

Mathieu Bourdenx, Aurélien Nioche, Sandra Dovero, Marie-Laure Arotcarena, Sandrine M. J. Camus, Gregory Porras, Marie-Laure Thiolat, Nicolas P. Rougier, Alice Prigent, Philippe Aubert, et al.

► To cite this version:

Mathieu Bourdenx, Aurélien Nioche, Sandra Dovero, Marie-Laure Arotcarena, Sandrine M. J. Camus, et al.. Identification of distinct pathological signatures induced by patient-derived α -synuclein structures in nonhuman primates. *Science Advances*, 2020, 6 (20), pp.eaaz9165. 10.1126/sciadv.aaz9165. hal-02611441

HAL Id: hal-02611441

<https://inria.hal.science/hal-02611441>

Submitted on 18 May 2020

HAL is a multi-disciplinary open access archive for the deposit and dissemination of scientific research documents, whether they are published or not. The documents may come from teaching and research institutions in France or abroad, or from public or private research centers.

L'archive ouverte pluridisciplinaire **HAL**, est destinée au dépôt et à la diffusion de documents scientifiques de niveau recherche, publiés ou non, émanant des établissements d'enseignement et de recherche français ou étrangers, des laboratoires publics ou privés.

1 Identification of distinct pathological signatures induced by patient-derived α - 2 synuclein structures in non-human primates 3 4

5 **Authors :** M. Bourdenx^{1,2,†,‡}, A. Nioche^{1,2,3,4,†}, S. Dovero^{1,2,†}, M.-L. Arotcarena^{1,2,†}, S. Camus^{1,2},
6 G. Porras^{1,2}, M.-L. Thiolat^{1,2}, N. P. Rougier^{1,2,5}, A. Prigent⁶, P. Aubert⁶, S. Bohic⁷, C. Sandt⁸, F.
7 Laferrière^{1,2}, E. Doudnikoff^{1,2}, N. Kruse⁹, B. Mollenhauer⁹, S. Novello^{10,11}, M. Morari^{10,11}, T. Leste-
8 Lasserre¹², I. Trigo Damas^{13,14}, M. Goillandeau^{1,2}, C. Perier^{14,15}, C. Estrada^{16,17}, N. Garcia-
9 Carrillo¹⁸, A. Recasens^{14,15}, N. N. Vaikath¹⁹, O. M. A. El-Agnaf¹⁹, M. Trinidad Herrero^{16,17}, P.
10 Derkinderen⁶, M. Vila^{14,15,20,21}, J. A. Obeso^{13,14}, B. Dehay^{1,2,* §} and E. Bezard^{1,2,*§}

11 **Affiliations:**

12 ¹ Univ. de Bordeaux, Institut des Maladies Neurodégénératives, UMR 5293, F-33000 Bordeaux, France;

13 ² CNRS, Institut des Maladies Neurodégénératives, UMR 5293, F-33000 Bordeaux, France;

14 ³ Institut Jean Nicod, Département d'études cognitives, ENS, EHESS, PSL Research University, 75005 Paris,
15 France;

16 ⁴ Institut Jean Nicod, Département d'études cognitives, CNRS, UMR 8129;

17 ⁵ INRIA Bordeaux Sud-Ouest, 33405 Talence, France;

18 ⁶ Inserm, U913, Nantes F-44035, France; Nantes University, Nantes F-44035, France; CHU Nantes, Department
19 of Neurology, Nantes F-44093, France;

20 ⁷EA-7442 Rayonnement Synchrotron et Recherche Médicale, RSRM, University of Grenoble Alpes, 38000
21 Grenoble, France ;

22 ⁸ SMIS beamline, Synchrotron SOLEIL, l'orme des merisiers, 91192 Gif sur Yvette, France;

23 ⁹Paracelsus-Elena-Klinik, Kassel, Germany; University Medical Center Goettingen, Institute of Neuropathology,
24 Goettingen, Germany;

25 ¹⁰Department of Medical Sciences, Section of Pharmacology, University of Ferrara, via Fossato di Mortara 17-
26 19, 44121 Ferrara, Italy;

27 ¹¹Neuroscience Center and National Institute of Neuroscience, University of Ferrara, via Fossato di Mortara 17-
28 19, 44121 Ferrara, Italy;

29 ¹²INSERM, Neurocentre Magendie, U1215, Physiopathologie de la Plasticité Neuronale, F-33000 Bordeaux,
30 France;

31 ¹³HM CINAC, HM Puerta del Sur and CEU-San Pablo University Madrid, E-28938 Mostoles, Spain;

32 ¹⁴Center for Networked Biomedical Research on Neurodegenerative Diseases (CIBERNED), Instituto Carlos III,
33 Spain;

34 ¹⁵Neurodegenerative Diseases Research Group, Vall d'Hebron Research Institute (VHIR)-Center for Networked
35 Biomedical Research on Neurodegenerative Diseases (CIBERNED), Barcelona, Spain;

36 ¹⁶Clinical and Experimental Neuroscience Unit, School of Medicine, Biomedical Research Institute of Murcia
37 (IMIB), University of Murcia, Campus Mare Nostrum, 30071 Murcia, Spain;

38 ¹⁷Institute of Research on Aging, School of Medicine, University of Murcia, 30071 Murcia, Spain;

39 ¹⁸Centro Experimental en Investigaciones Biomédica (CEIB), Universidad de Murcia, Murcia, Spain;

41 ¹⁹Neurological Disorders Research Center, Qatar Biomedical Research Institute (QBRI), Hamad Bin Khalifa
42 University (HBKU), Education City, Qatar;

43 ²⁰Department of Biochemistry and Molecular Biology, Autonomous University of Barcelona (UAB), Barcelona,
44 Spain;

45 ²¹Catalan Institution for Research and Advanced Studies (ICREA), Barcelona, Spain.
46

47 *To whom correspondence should be addressed to: Dr. Benjamin Dehay and to Dr. Erwan Bezar, Institute of
48 Neurodegenerative Diseases, Université de Bordeaux, CNRS UMR 5293, Centre Broca Nouvelle-Aquitaine, 146
49 rue Léo Saignat, 33076 Bordeaux cedex, France. E-mail: benjamin.dehay@u-bordeaux.fr (B.D.) and
50 erwan.bezard@u-bordeaux.fr (E.B.)

51 † These authors contributed equally to this work

52 § BD and EB are co-last authors

53 ‡ Present address: Albert Einstein College of Medicine. Department of Developmental and Molecular Biology.
54 1300 Morris Park Ave. Bronx, NY, 10461, USA.

55

56

57

58

59

60

61

62

63

64

65

66

67

68

69

70

71

72

73 **ABSTRACT**

74 Dopaminergic neuronal cell death, associated with intracellular α -synuclein (α -syn)-rich protein
75 aggregates (termed ‘Lewy bodies’), is a well-established characteristic of Parkinson’s disease.
76 Much evidence, accumulated from multiple experimental models has suggested that α -syn plays a
77 role in PD pathogenesis, not only as a trigger of pathology but also as a mediator of disease
78 progression through pathological spreading. Here we have used a machine learning-based approach
79 to identify unique signatures of neurodegeneration in monkeys induced by distinct α -syn pathogenic
80 structures derived from PD patients. Unexpectedly, our results show that, in non-human primates,
81 a small amount of singular α -syn aggregates is as toxic as larger amyloid fibrils present in the LBs,
82 thus reinforcing the need for preclinical research in this species. Furthermore, our results provide
83 evidence supporting the true multifactorial nature of PD as multiple causes can induce similar
84 outcome regarding dopaminergic neurodegeneration.

85

86

87 **INTRODUCTION**

88

89 The seminal work of Braak and colleagues suggesting that Lewy body (LB) pathology follows a
90 predictable pattern of progression within the brain in Parkinson's disease (PD) (1) as well as the
91 'host-to-graft' observation (2-4) led to the development of experimental models based on injection
92 with α -synuclein (α -syn – the primary protein component of LB) assemblies (5-7). These
93 experimental models suggest that α -syn, in pathological conformations such as the one found in
94 LBs, initiates a cascade of events leading to dopaminergic neuron degeneration as well as cell-to-
95 cell propagation of α -syn pathology through a self-templating mechanism.

96 Several studies have suggested that pre-fibrillar oligomers may represent one of the major
97 neurotoxic entities in PD (8, 9). This notion has been derived primarily from studies using large
98 doses of recombinant α -syn applied to cell cultures or injected into adult mice, over-expressing
99 either mutant or wild-type α -syn (10). In agreement with these findings, we have shown that
00 intracerebral injection of low doses of α -syn-containing LB extracts, purified from the substantia
01 nigra, pars compacta (SNpc) of postmortem PD brains, promotes α -syn pathology and
02 dopaminergic neurodegeneration in wild-type mice and non-human primates (11). Importantly, this
03 neuropathological effect was directly linked to the presence of α -syn in LB extracts, since immuno-
04 depletion of α -syn from the LB fractions prevented the development of pathology following
05 injection into wild-type mice.

06 In this study, our aim was to thoroughly investigate this experimental model of synucleinopathy in
07 non-human primates. The initial study design was to administrate fractions derived from the same
08 PD patients containing either soluble and small α -syn aggregates (hereafter named noLB) or LB-
09 type aggregates (hereafter named LB). However, because of the unexpected finding that non-
10 human primates, unlike mice, are susceptible to soluble or finely granular α -syn, we sought to
11 elucidate the response characteristics induced by either LB or noLB fractions. To achieve a
12 thorough analysis of these α -syn-related characteristics, we took advantage of the strength of
13 machine-learning algorithms for discovering fine patterns among complex sets of data and
14 developed a new method compatible with the constraints of experimental biology. We here report
15 the identification of primate-specific responses to selected α -syn assemblies associated with
16 different pathogenic mechanisms. Overall, our results support the concept of the multifactorial
17 nature of synucleinopathies.

18

19

20 RESULTS

21 *Purification and characterization of α -synuclein extracts from PD patients*

22 NoLB and LB fractions were obtained from the SNpc of five sporadic PD brains exhibiting
23 conspicuous LB pathology. The samples were processed through differential ultracentrifugation in
24 a sucrose gradient, and analyzed for the presence of α -syn aggregates by filter retardation assay
25 (Fig. 1A) (11). Further characterization of noLB and LB fractions was performed by co-localization
26 of α -syn and the amyloid dye Thioflavin S (Fig. 1B) as well as ultrastructural examination by
27 electron microscopy (Fig. 1C). These assays confirmed the presence of misfolded α -syn in both
28 fractions. We also performed biochemical characterization of the stability of assemblies after
29 proteinase K digestion (Fig. 1D) and detergent treatments (Fig. 1E) followed by α -syn dot-blot
30 assays. While total α -syn content was comparable between selected fractions (as measured by α -
31 syn ELISA), LB fractions showed higher resistance to proteinase K treatment (noLB
32 $t_{1/2}$ =15.23minutes vs LB $t_{1/2}$ >60minutes) (Fig. 1D) as well as greater resistance to multiple
33 detergents, including 8M Urea (Fig. 1E). We then measured the content of α -syn aggregates using
34 human α -syn aggregation TR-FRET-based immunoassay, which revealed a significantly higher
35 amount of aggregated α -syn in LB fractions (Fig. 1F). To obtain insight into the content of
36 monomeric and aggregated α -syn within noLB and LB fractions of PD patients, sarkosyl treatment
37 was applied to both fractions to induce physical separation, and then velocity sedimentation and
38 density floatation gradients were performed to quantify these two respective populations and
39 determine their relative abundance in each fraction (Fig. S1 A-H). Strikingly, while LB fractions
40 contained ~90% of aggregated α -syn, noLB fractions were composed of ~10% of this pathological
41 form of the protein (Fig. S1 I). Also, in order to confirm the quality of the LB extraction, we
42 performed a filter retardation assay which showed that LB fractions, but not noLB fractions, were
43 highly enriched in known components of LBs, such as phosphorylated S129 α -syn, ubiquitin, p62,
44 hyperphosphorylated tau and A β (Fig. S2 A).

45 Micro-Infrared Spectroscopy of LB and noLB fractions was performed to show conformational
46 changes in amyloid structures at the molecular level (Fig. S2 B-E) and this confirmed the presence
47 of β -sheet structures in both assemblies (Fig. S2 B-C). Although their velocity of sedimentation
48 and density floatation characteristics were similar, the aggregates present in the LB and noLB
49 fractions were different in nature based upon the evidence of Micro-Infrared Spectroscopy.
50 Principal component analysis (PCA) showed that, in the LB fractions, large aggregates
51 corresponding to the major pieces of LB were present (Fig. S2D, cluster on the right). PCA further
52 showed that, in the range of 1,590-1,700 cm^{-1} , the LB group contained a fraction of amyloid

53 aggregates with different amyloid structures from those in the noLB group as they clearly
54 segregated by PCA in two clusters (Fig. S2 D-E). Altogether, these results suggest that while LB
55 fractions primarily contained large aggregated α -syn fibrils, noLB fractions contained soluble α -
56 syn and a smaller enrichment of α -syn aggregates featuring a specific amyloid structure not found
57 in the LB fractions.

58 Data from several studies suggest that both recombinant α -syn preformed fibrils (12-14) and
59 patient-derived α -syn (11) can promote pathogenic templating of endogenous α -syn ultimately
60 leading to dopaminergic neurodegeneration in SNpc. Following quantification by ELISA, both
61 mixes of fraction were diluted to ~ 24 pg α -syn per microliter. Then, those fractions were tested for
62 their pathogenic effects on TH-positive dopaminergic neurons in primary mesencephalic cultures
63 (Fig. S3 A) as well as *in vivo* in wild-type mice. Four months after supranigral injection, LB-injected
64 mice displayed, as expected, significant dopaminergic degeneration, while noLB injections in mice
65 had no impact on dopaminergic neurons (Fig. 1G-H) as we have previously reported for other
66 SNpc-derived LB fractions (11), thus validating the toxicity of the preparation prior to injection
67 into non-human primates.

68

69 *Intrastriatal injection of LB and noLB fractions from Parkinson's disease patients induces*
70 *nigrostriatal neurodegeneration in baboon monkeys*

71 To determine the mechanisms of α -syn aggregates toxicity in a species closer to humans, adult
72 baboon monkeys (n=4-7 per experimental group) received bilateral stereotaxic injections (100 μ l)
73 of either LB or noLB fractions into the putamen before euthanasia 24 months post-injection. This
74 time-frame was chosen based on our previous studies indicating that after 14 months post-injection,
75 ongoing pathogenic effects can already be measured, and was extended to potentially reach disease-
76 relevant lesions. Two years after administration, LB-injected monkeys displayed significant striatal
77 dopaminergic terminal loss both in the putamen and in the caudate nucleus, accompanied by a
78 significant decrease in tyrosine hydroxylase (TH) immunoreactivity in the substantia nigra pars
79 compacta (SNpc) (Fig. 2). Stereological counts showed that LB-injected animals exhibited TH-
80 positive and Nissl-positive cell loss in the SNpc (16% and 23%, respectively). No overt
81 parkinsonism was observed, however, since the extent of the lesion remained below the threshold
82 for symptom appearance; i.e. 45% of cell loss (15), compared to an age-matched control group.

83 At odds with mice either generated for the purpose of this study (Fig. 1G-H), previously published
84 (11), or produced in the context of other in-house studies (data not shown), noLB-injected monkeys
85 showed degeneration of the nigrostriatal pathway including dopaminergic cell loss (i.e. 16% of TH-

86 positive neurons and 28% of Nissl-positive neurons quantified by stereology), similar to that
87 observed in LB-injected monkeys (Fig. 2). Facing such an unexpected finding, we aimed to identify
88 specific characteristics of the pathological mechanisms involved in α -syn toxicity induced by each
89 fraction independently, using a large-scale approach in combination with machine learning for
90 pattern identification.

91

92 *Machine-learning algorithm predicts nigrostriatal degeneration*

93 We performed an exploratory approach and aimed to distinguish relevant variables allowing
94 accurate prediction of neurodegeneration (i.e., to operate a feature selection). Overall, we
95 investigated a large number of variables tapping on behavioral, histological, biochemical,
96 transcriptional and biophysical approaches (Fig. 3A) applied to several brain areas (n=40 – Fig.
97 3B), totalizing 180 variables measured for each individual (Fig. S4A for variable abbreviation
98 nomenclature; Table S1 for exhaustive list of variables; Table S2 features all raw data). We first
99 extracted from this dataset, every variable that actually quantified neurodegeneration (i.e.
00 dopaminergic markers such as TH or dopamine transporter by immunohistochemistry), ending up
01 with 163 variables per animal.

02 Then, to operate feature selection, we designed a distributed algorithm using multiple layer
03 perceptron (MLP) (Bourdenx and Nioche, 2018), a classic machine-learning algorithm based on
04 artificial neural network that is able to approximate virtually any functions (Hornik et al., 1989).
05 This algorithm was given, as input, the data obtained for each animal for the 163 aforementioned
06 variables and its output is a rank of these variables regarding their ability to predict three indicators
07 of dopaminergic tract integrity; that were levels of tyrosine hydroxylase staining in (i) the SNpc,
08 (ii) the putamen and (iii) the caudate nucleus.

09 The main difficulty was to overcome the large number of input variables (163) compared to the
10 sample size (n=4-7 per group), which can induce a selection and reporting bias (Kuncheva and
11 Rodriguez, 2018). In order to tackle this “p > n” problem, instead of using a single network that
12 could be prone to overfitting, we put in competition several networks.

13 Each MLP was composed of a single hidden layer of 3 neurons (Fig. 3C). It has as input a subset
14 of 3 variables (out of the 163) and as output the 3 indicators of dopaminergic tract integrity. In total,
15 we used 708,561 sets of 3 inputs variables. Every instance of MLP was trained with 80% of our
16 sample (always a combination of control and injected animals) and tested on the remaining 20%.
17 The performance of each set of 3 input variables was evaluated according to the difference between
18 the predicted values of TH staining and the actual ones.

19 We focused on the top 1% of the best networks and counted the occurrence of each of the 163
20 variables in the subset of 3 variables used by these best networks (Fig. 3C). We ranked each variable
21 according to the number of occurrences (Fig. 3C) for LB- (Fig. 3D) and noLB-injected animals
22 (Fig. 3E) independently.

23 In order to avoid possible overfitting, we used several methods in combination. First, we performed
24 cross-validation by splitting the dataset into two parts: a training and a testing set of data. 80% of
25 the data were randomly selected to train the networks (and independently for each network), while
26 the 20% remaining were used to evaluate the networks. Then, in order to evaluate the robustness of
27 the quality of prediction for a given set, we repeated this cross-validation step 50 times for every
28 set of 3 input variables (each network was trained and tested using a different partition of the dataset
29 - total number of network: 35,428,050). Lastly, we generated random data and used them as input
30 for the MLP. As expected, performances were significantly lower compared to our actual dataset
31 (Fig. S4B, C).

32 Overall, this unique approach allowed us to rank input variables according to their explanatory
33 power and therefore to extract the strongest predictors of neurodegeneration for each experimental
34 group. Interestingly, despite similar levels of nigrostriatal degeneration between LB- and noLB-
35 injected animals (Fig. 2B), the algorithm allowed us to identify differential variable sorting patterns
36 (Fig. 3D-E).

37

38 *MLP-derived signatures can identify unique characteristics between experiment group*

39 Next, we compared the LB and noLB characteristics using the rank-rank hypergeometric overlap
40 (RRHO) test (Fig. 4A). Interestingly, low similarity was observed for the highly ranked variables
41 suggesting specific differences in the biological response to the injection of LB or noLB (Fig. 4B).
42 Focusing on the 20 first variables that showed low similarity between groups, we found that LB-
43 exposed monkeys were characterized by both quantitative and qualitative changes in α -syn levels
44 (i.e. phosphorylation at Ser129 and aggregation) especially in cortical areas corroborated by distinct
45 methodologies as well as by a dysfunctional equilibrium in neurochemistry of basal ganglia output
46 structures classically associated with parkinsonism (16, 17) (Fig. 4C – Fig. S5). Conversely, noLB-
47 exposed monkeys exhibited more diverse nigrostriatal-centric characteristics with variables related
48 to α -syn aggregation, proteostasis and Zn homeostasis (Fig. 4D - Fig. S6). Together, we identified
49 specific properties for both groups with limited overlap (35% - 7/20 variables) for an identical level
50 of degeneration.

51

52 *Retrospective literature search validates MLP derived signatures*

53 We next used a retrospective analysis to validate the relevance of the MLP-derived signature in
54 PD. Although, some variables have never been investigated in the context of PD, others have been
55 studied and reports exist in the literature. For instance, the amount of phosphorylated Ser129 α -
56 synuclein in the entorhinal (*h.psyn.ctx.er.ant*) and parahippocampal (*h.psyn.ctx.phipp*) cortex - 1st
57 and 2nd best predictors for the LB group – have been already associated with PD pathology. Studies
58 of post-mortem brains from PD patients revealed the presence of LB in these regions which was
59 correlated with disease progression (18) and predicted cognitive deficit in PD patients (19).
60 Interestingly, the anterior entorhinal cortex has also been shown to be affected by severe α -syn
61 pathology, related to olfactory dysfunction in prodromal phases of PD pathology (20). In addition,
62 increased levels of phosphorylated Ser129 α -syn in sensorimotor (*h.syn.ctx.sma.ant*) and
63 cingulate cortices (*h.syn.ctx.cg.ant*), shared by both LB and noLB signatures, have already been
64 reported by our group in an independent cohort of non-human primates (11).

65 Both LB and noLB signatures, and especially noLB, showed that variables related to α -syn
66 aggregation status were among the best predictors (LB: 1 in top10 best predictors; noLB 3 in top10
67 best predictors). This was highly expected from the literature as α -syn aggregation has been
68 associated with PD pathology (21).

69 Variables related to the proteostasis network (levels of the lysosomal receptor LAMP2 –
70 *wb.lamp2.sn* - 6th or amount of ubiquitinated proteins – *wb.ub.sn* – 9th) were more specifically
71 associated with the noLB signature. This is of high interest as proteostasis defect is more and more
72 considered as a key step in pathogenicity (22-24).

73 Levels of the microglia marker, Iba1, was ranked as the third best predictor of neurodegeneration
74 in the LB signature. Microglial inflammatory response was shown to be implicated in
75 neurodegeneration in many animal models, including α -syn overexpressing and toxin-based animal
76 model of PD (25).

77 Lastly, *postmortem* analysis of Zn²⁺ concentration in the brains of PD patients has shown elevated
78 levels in the striatum and SNpc (26). Conversely, a recent meta-analysis showed a decrease of
79 circulating Zn²⁺ levels in PD patients (27). In experimental models of PD, Zn²⁺ accumulation has
80 been associated with dopaminergic degeneration in rodent exposed to mitochondrial toxins (28,
81 29).

82 83 *Experimental confirmation of MLPs' prediction*

84 We aimed to confirm the relevance of the top first MLP selected variables. Since the LB signature
85 was associated with changes in α -syn phosphorylation in cortical areas, we analyzed side-by-side
86 the levels of α -syn and phosphorylated Ser129 α -syn in 18 brain regions (Fig. 5A). Interestingly,

87 in agreement with the LB signature obtained from the MLP, LB-injected monkeys displayed a
88 stronger accumulation of phosphorylated Ser129 α -syn compared to noLB-injected animals (Fig.
89 5A-B). Also, the 2 most enriched variables of the LB signature (i.e. phosphorylated α -syn levels in
90 parahippocampal and entorhinal cortices (Fig. 4C)) showed significant negative correlations with
91 degrees of degeneration (Fig. 5C-D), thus confirming their ability to predict neurodegeneration.
92 Then, we decided to confirm the relevance of one of the strongest predictors, the levels of Zn^{2+} in
93 the SNpc in independent experiments. First, we observed a significant increase of Zn^{2+} in noLB-
94 injected mice compared to sham-injected or LB-injected mice (Fig. S7A). Second, we analyzed the
95 levels of Zn^{2+} in LB-injected macaque monkeys from a previous study of our laboratory (11).
96 Interestingly, despite the fact that these experiments were done in a different non-human primate
97 sub specie, injection of LB in the putamen (similar to the present study) or above the SNpc (different
98 from the present study) induced elevation of Zn^{2+} levels in the SNpc, as measured by SR-XRF (Fig.
99 S7B). Of note, the dimension of the effect was similar across studies (Fig. S7E). Then, to
00 understand whether that modulation Zn^{2+} levels was specific to our experimental paradigm, we
01 measured Zn^{2+} levels in the context of adeno-associated virus-mediated overexpression of mutant
02 human α -syn in both rats and marmoset monkeys (30) using the same methodology (Fig. S7C, D).
03 Here, overexpression of α -syn did not triggered accumulation of Zn^{2+} in the SNpc (despite inducing
04 dopaminergic neurodegeneration – (30) suggesting that this phenomenon is specific to seeding
05 experiment paradigms.

06 Lastly, we analyzed a publicly available cortical proteomic database of healthy individual and PD
07 patients. Of interest, we observed that several Zn^{2+} transporters were elevated in the brains of PD
08 patients thus suggesting a zinc dyshomeostasis in patients (Fig. S7F). Indeed, plasma membrane
09 transporters such as the zinc transporter 1 (ZnT1), the Zrt-/Irt-like protein 6 (ZIP6) and ZIP10
10 showed increased levels (Fig. S7G-I) while the synaptic vesicle membrane transporter ZnT3
11 remained constant (Fig. S7J).

12

13 *Association metric shows independence of strong predictors*

14 As we used combinations of 3 variables and because of the structure of MLPs, one could expect
15 that some combinations would complement each other to allow finer prediction of
16 neurodegeneration levels. To address this question, we used a classic measurement of association
17 in the field of data-mining: lift (31) and plotted the results as network plots showing association
18 (edge size) and enrichment in the best learners (node size). Lift calculation was corrected for error
19 prediction to avoid detrimental association between variables. The first observation was that the

20 most enriched variables (top 3 to 5) appeared to be self-sufficient to predict the neurodegeneration
21 levels with minimal error (Fig. 6). Some variables, with modest enrichment, showed strong positive
22 associations that were specific to each experimental group. Associated variables in LB-injected
23 monkeys were: (i) α -syn-related parameters along the SNpc-striatum-cortex axis, an impairment of
24 locomotion and the ethologically-defined orientation of the animals towards their environment (Fig.
25 6 top left inset); (ii) oligomeric α -syn species measured in the midbrain and striatum equally
26 associated, but to lesser extent, with α -syn levels in cortex and plasma (Fig. 6 top right inset).
27 In noLB-injected animals, the analysis shed light upon the relative abundance of two members of
28 the macroautophagy pathway (Fig. 6B top left) as well as the balance between monomeric and high-
29 molecular weight species of α -syn in the putamen (Fig. 6B bottom right). Such disruption of the
30 nigrostriatal pathway has repercussions upon the basal ganglia physiology as GABA levels in their
31 output structure, the internal globus pallidus, was associated with a decreased social behavior (Fig.
32 6B bottom left inset).

33

34 **DISCUSSION**

35 In the present study, we report that, in non-human primates, injection of distinct α -syn assemblies
36 derived from PD patients lead to dopaminergic degeneration through discrete mechanisms.
37 Applying a machine-learning method, we gained insight into unique signatures of degeneration
38 induced by injection of two distinct α -syn pathogenic assemblies (i.e. those contained in the LB
39 and noLB fractions derived from idiopathic PD patients' brains). To do so, we built a large dataset
40 with 180 variables obtained from behavioral, histological, biochemical, transcriptional and
41 biophysical approaches applied to several brain areas for each individual. By using a distributed
42 MLP algorithm that we developed for the purpose of this study, we identified characteristics that
43 give insight into the strongest predictors of neurodegeneration for each experimental group. We
44 have, therefore, described for the first time that distinct α -syn assemblies leading to similar
45 degeneration in monkeys are associated with different mechanisms, hence experimentally
46 confirming the true multifactorial nature of synucleinopathies.

47 Our results illustrate that both small oligomeric as well as larger α -syn assemblies induce
48 dopaminergic degeneration in non-human primates. This finding was unexpected, since previous
49 mouse studies from our laboratory showed that noLB injection did not have any observable
50 consequence regarding dopaminergic degeneration, α -syn accumulation or phosphorylation (11).
51 In agreement, other groups also showed the absence of toxicity of soluble recombinant α -syn (12).

52 One possible explanation is that primate dopaminergic neurons could be highly susceptible to α -
53 syn toxicity. This could be in part due to their unique cellular architecture (32), a feature already
54 known to contribute to the selective vulnerability of these neurons in PD (33). In fact, the large and
55 complex axonal arbor of dopamine neurons make them particularly vulnerable to factors that
56 contribute to cell death and, in primates, this axonal arbor is ten-fold the size of that in rodents
57 (32). In addition, primate dopamine neurons display unique molecular characteristics (e.g. the
58 presence of neuromelanin, the intracellular levels of which have been shown to be important in the
59 threshold for the initiation of PD) (34). These unique features of primate dopaminergic neurons
60 might be important in explaining the toxic mechanisms of the relatively low content of α -syn
61 aggregates in the noLB fractions. Additional studies are now needed to fully address the question
62 of host-seed interactions, but our results highlight the relevance and the need of the non-human
63 primate model for the study of synucleinopathies.

64 We also confirmed that the toxicity mechanisms associated with patient-derived α -syn aggregates
65 are shared features among patients and, therefore, common to the disease. Indeed, LB and noLB
66 fractions used in this study were isolated from a pool of 5 patients who were different from the pool
67 of 3 patients used in our previous study in mice (11). In the mice experiment (Fig. S3B) performed
68 in this study, we observed the same level of dopaminergic degeneration (~40% at 4 months after
69 injection).

70 The surprising observation, in non-human primates, that the noLB fraction is toxic to the same
71 extent as the LB fraction suggests the existence of previously unrecognized forms of α -syn toxicity.
72 Several studies have suggested that pre-fibrillar oligomeric species are the toxic α -syn species (8,
73 9). Our biochemical studies showed that noLB and LB fractions had different amyloid properties
74 (Fig. 1), contents (Fig. S1, S2A) and structures (Fig. S2B-E). Indeed, LB fractions contained a
75 majority of large aggregated α -syn fibrils as well as some smaller aggregates while noLB fractions
76 contained a smaller proportion (10 folds) of smaller aggregates and soluble α -syn. More
77 importantly, the smaller aggregates were different in nature between LB and noLB fractions, as
78 shown by micro-infrared spectroscopy (Fig. S2B-E). One could hypothesize that the observed effect
79 is due to a species common between LB and noLB. However, because of the extent of degeneration,
80 which was similar between the two experimental groups, and the α -syn content dissimilarity, both
81 in amount and nature, this appears very unlikely. We believe that our results support the notion of
82 the existence of a range of α -syn pathogenic structures with distinct toxic properties within the PD
83 brain. Further work is necessary to provide a complete structural characterization of those species.
84 As yet, very few studies report the high-resolution structures of α -syn aggregates, which are on the

85 one hand, only derived from studies using recombinant α -syn and, on the other hand, limited to
86 near atomic resolution (35-37). Encouragingly, much effort is currently being devoted to this field
87 of research and two recent studies reported the atomic structure of α -syn fibrils determined by cryo-
88 electron microscopy (38, 39), while still being limited to recombinant-generated α -syn, and not
89 isolated from human brain tissue.

90 In order to perform a characterization of the effects of the two fractions, we developed a machine
91 learning method to identify their biological characteristics. It is now well accepted that machine
92 learning algorithms can be trained to detect patterns as well as, or even better than, humans (40-
93 42). Instead of the classification algorithms (the algorithm learns to identify in which category a
94 sample belongs) that were mostly used in recent applications of machine learning in biology (43),
95 we chose in this study to predict continuous and biologically-relevant variables using MLPs. Our
96 choice was motivated by the limited sample size that is often a constraint of experimental biology.
97 Although it might have been possible to use other feature selection methods, the use of MLPs with
98 a distributed architecture allowed us to avoid overfitting issues and to develop a method particularly
99 well-suited for low sample size datasets (44). As both LB and noLB-injected monkeys displayed
00 similar levels of degeneration, they were indistinguishable using that endpoint. Instead of using a
01 clustering analysis or a classification method, hence making the *a priori* assumption that these
02 groups were different, we preferred to submit the two experimental groups to the MLP
03 independently.

04 The combination of this constrained, distributed architecture and the holistic approach allowed us
05 to rank input variables according to the number of times they appeared in the group of best
06 predictors (defined as top 1% of best networks). A major issue in the use of machine learning in
07 experimental biology in the 'black-box' is the fact that it is usually impossible to 'understand' how
08 an algorithm predicted an output (45). By using a reverse engineering method, we aimed to tackle
09 that issue. Because we explored all possible combinations of our variables, we could rank the input
10 variables assuming that the more they appeared in the top 1%, the more they contained information
11 allowing precise prediction of the neurodegeneration levels. Interestingly, our two experimental
12 groups showed that some of the best predictors were similar (about 30%) but the majority were
13 different. One could hypothesize that the similar variables between the two signatures probably
14 embedded information that are consequences of neurodegeneration while the different ones
15 probably contain information regarding the process of disease initiation and/or progression. Further
16 experimental studies are now needed to confirm the relevance of these variables.

17 Also, as these two kinds of α -syn assemblies were associated with different signatures identified
18 by our MLP approach, we propose that our results illustrate the multifactorial nature of the disease
19 as different mechanisms (i.e. signatures) initiated by different triggers (i.e. α -syn assemblies) led
20 to similar consequences (i.e. degeneration levels).

21 Using this methodology, we confirmed the interest of highly-expected variables but more
22 importantly also unexpected variables that appear to be excellent predictors of α -syn-associated
23 dopaminergic degeneration. The first hit for LB-injected animals was phosphorylated α -syn in the
24 entorhinal cortex (as we have previously shown) followed by phosphorylated α -syn in the para-
25 hippocampal cortex (unexpected), striatal microglial activation and GABA dysregulation in the
26 internal part of the globus pallidus (expected) (Fig. S5). Conversely, Zn homeostasis was a strong
27 predictive variable (unexpected) followed by α -syn aggregation-related terms (expected) in noLB-
28 injected animals (Fig. S6).

29 In order to confirm the prediction made by the MLP approach, we first performed a retrospective
30 literature analysis. This analysis showed that a significant part of the best predictors has been shown
31 in the literature to be correlated with disease progression. Then, we attempted to confirm the interest
32 of one of the top hits, the accumulation of Zn^{2+} in the SNpc, in independent experimental cohorts.
33 Interestingly, we here describe that both in mice injected with noLB or in macaque monkeys (a
34 different non-human primate sub species that the baboons used in that study) injected either in the
35 striatum or in the SNpc, Zn levels were increased in the SNpc. However, in mice, Zn
36 dyshomeostasis was not associated with neurodegeneration in the noLB group (at odds with what
37 was observed in monkeys) suggesting a species difference in the relationship between zinc levels
38 and dopaminergic tract integrity. Surprisingly, that result was not observed in rats and marmoset
39 monkeys overexpressing human mutant α -syn. This observation might suggest that Zn
40 dyshomeostasis is a feature of disease not triggered in the context of human mutant α -syn
41 overexpression that is associated with fast progressing pathology (Bourdenx et al. 2015). Then, in
42 order to expand our results to human pathology, we analyzed a publicly available proteomic dataset
43 of human samples. According to that analysis, PD patients displayed increased levels of plasma
44 membrane Zn transporters, hence suggesting a Zn dyshomeostasis in patients. In the context of PD,
45 Zn dyshomeostasis has been associated with autophagy/lysosomal dysfunction in the context of
46 *PARK9* mutations (Ramirez et al. 2006, Dehay et al. 2012). Further studies are now needed to fully
47 unravel this connection.

48 Altogether, our findings show that primate dopaminergic neurons are sensitive to both small, mostly
49 soluble, α -syn extracts as well as larger, aggregated, α -syn extracts derived from PD patients. These

50 findings involve two immediate outcomes. First, since this toxicity has not been reported so far it
51 suggest species differences that would need to be thoroughly investigated (46, 47) and calls for a
52 systematic appraisal of proteinopathies in primates in particular for validating therapeutic strategies
53 before clinical testing (48). Second, the present study highlights the complex structure-toxicity
54 relationship of α -syn assemblies and corroborates the multifactorial origin of synucleinopathies as
55 distinct assemblies can induce similar degeneration (that would probably lead to similar clinical
56 manifestation in patients) through different mechanisms, nigrostriatal or extranigral brain
57 pathways, calling for molecular diagnosis to identify patient sub-populations before launching
58 large-scale, heterogeneous in nature, clinical trials. Finally, we developed a machine-learning
59 approach allowing and quantitative assessment of the explanatory power of a given set of variables
60 compatible with the constrained sample size of experimental biology.

61

62

63 MATERIALS AND METHODS

64 Access to data and machine-learning code for replicability and further use by the community

65 The entire raw data set is made available to the readers (Table S2). Authors chose not to provide
66 representative examples of each procedure for the sake of space and because the entire data set is
67 fully disclosed. Further information and requests for examples should be directed to and will be
68 fulfilled by the Corresponding Contacts. Hyperlink to the machine-learning code
69 (10.5281/zenodo.1240558) is provided (<https://zenodo.org/record/1240558#.XC8pqy17Su4>).

71 Ethics statement

72 Experiments were performed in accordance with the European Union directive of September 22,
73 2010 (2010/63/EU) on the protection of animals used for scientific purposes. The Animal
74 Experimentation Ethical Committee (CEEA) of the Vall d'Hebron Institute of Research (VHIR)
75 approved experiments under the license number CEEA 81/13 (rats). The Institutional Animal Care
76 and Ethical Committee of Bordeaux University (CE50, France) approved experiments under the
77 license number 5012099-A (mice). The Institutional Animal Care and Ethical Committee of Murcia
78 University (Spain) approved experiments under the license number REGA ES300305440012
79 (monkeys).

81 Animals and Stereotactic Injections

82 *Mice.* Wild-type C57BL/6 mice (4 months old) received 2 μ l of either LB fractions or noLB
83 fractions by stereotactic delivery to the region immediately above the right substantia nigra
84 (coordinates from Bregma: AP=-2.9, L= -1,3, DV=-4.5) at a flow rate of 0.4 μ l/min and the pipette
85 was left in place for 5 min after injection to avoid leakage. Mice were killed four months after
86 injection. Ten to fifteen mice were used in each group.

87 *Monkeys.* Animals, which were from the research animal facility of the University of Murcia
88 (Murcia, Spain) and housed in 2 multi-male multi-female exterior pens, were studied in a breeding
89 farm over 2 years (Murcia, Spain). Animals were fed fruits, vegetables and monkey pellets twice a
90 day before 9 am and after 5pm. Water was available ad libitum. 17 healthy adult olive baboons
91 (*Papio papio*) were used in this study. Group sizes were chosen assuming a one-tailed alpha of 0.05,
92 with sample size of at least three per group, which provided >80% power to detect a difference
93 between the treatment groups and the control group, using a Fisher's exact test. Animals were
94 randomized into treatment or control groups. Six baboons were used for LB injections, four were
95 used for noLB injections and seven were untreated control animals. Intrastratial injections of either

96 LB fractions or noLB fractions were performed at 2 rostrocaudal levels of the motor striatum
97 (anterior commissure [AC], -1mm and -5mm) under stereotactic guidance as previously described
98 (49-52). The total injected volume per hemisphere was 100 μ l (2 injection sites with 50 μ l each at
99 3 μ l/min at each location site). After each injection, the syringe was left in place for 10 min to
00 prevent leakage along the needle track. A number of parameters were monitored during the course
01 of the two-year study, including survival and clinical observations. At the end of the experiment
02 (24 months post-injection), all monkeys were euthanised with pentobarbital overdose (150mg/kg
03 i.v.), followed by perfusion with room-temperature 0.9% saline solution (containing 1% heparin)
04 in accordance with accepted European Veterinary Medical Association guidelines. Brains were
05 removed quickly after death. Each brain was then dissected along the midline and each hemisphere
06 was divided into three parts. The left hemisphere was immediately frozen by immersion in
07 isopentane at -50°C for at least 5 min and stored at -80°C. The right hemisphere was fixed for one
08 week in 10 vol/tissue of 4% paraformaldehyde at 4°C, cryoprotected in two successive gradients of
09 20 then 30% sucrose in phosphate buffered saline (PBS) before being frozen by immersion in
10 isopentane (-50°C) for at least 5 min and stored at -80°C until sectioning. CSF and blood samples
11 (plasma, serum, whole blood) in the 17 animals were carefully collected before euthanasia. No
12 samples were excluded from analysis in these studies.

13

14 **Purification of Lewy bodies from human PD Brains**

15 The samples were obtained from brains collected in a Brain Donation Program of the Brain Bank
16 “GIE NeuroCEB” run by a consortium of Patients Associations: ARSEP (association for research
17 on multiple sclerosis), CSC (cerebellar ataxias), France Alzheimer and France Parkinson. The
18 consents were signed by the patients themselves or their next of kin in their name, in accordance
19 with the French Bioethical Laws. The Brain Bank GIE NeuroCEB (Bioresource Research Impact
20 Factor number BB-0033-00011) has been declared at the Ministry of Higher Education and
21 Research and has received approval to distribute samples (agreement AC-2013-1887). Human
22 SNpc was dissected from fresh frozen postmortem midbrain samples from 5 patients with sporadic
23 PD exhibiting conspicuous nigral LB pathology on neuropathological examination (mean age at
24 death: 75 ± 2.75 years; frozen post-mortem interval: 31.8 ± 7.45 h; GIE Neuro-CEB BB-0033-
25 00011). Tissue was homogenized in 9 vol (w/v) ice-cold MSE buffer (10 mM MOPS/KOH, pH 7.4,
26 1M sucrose, 1mM EGTA, and 1mMEDTA) with protease inhibitor cocktail (Complete Mini;
27 Boehringer Mannheim) with 12 strokes of a motor-driven glass/teflon dounce homogenizer. For
28 LB purification, a sucrose step gradient was prepared by overlaying 2.2 M with 1.4 M and finally
29 with 1.2 M sucrose in volume ratios of 3.5:8:8 (v/v). The homogenate was layered on the gradient

30 and centrifuged at 160,000 x g for 3 h using a SW32.1 rotor (Beckman). Twenty-six fractions of
31 1500 μ l were collected from each gradient from top (fraction 1) to bottom (fraction 26) and analyzed
32 for the presence of α -synuclein aggregates by filter retardation assay, as previously described (11).
33 Further characterization of LB fractions was performed by immunofluorescence, α -synuclein
34 ELISA quantification and electron microscopy as previously described (11). For stereotactic
35 injections, LB-containing fractions from PD patients were mixed together in the same proportion
36 (PD#1, fractions 19 and 20; PD#2, fractions 19 and 20; PD#3, fraction 22; PD#4, fractions 17,18
37 and 19; PD#5, fractions 20, 21 and 23). NoLB-containing fractions (i.e. fraction 3, at the beginning
38 of the 1,2M interface) derived from the same PD patients (which contain soluble or finely granular
39 α -synuclein) but lacks large LB-linked α -synuclein aggregates were obtained from the same sucrose
40 gradient purification. Using enzyme-linked immunosorbent assay (ELISA) kit against human α -
41 synuclein (Invitrogen, #KHB0061 – following manufacturer’s recommendations), α -syn
42 concentration was measured and both LB and noLB fractions were adjusted to ~24 pg α -synuclein
43 per microliter. In all cases, samples were bath-sonicated for 5 min prior to *in vitro* and *in vivo*
44 injections.

45 46 **Characterization of noLB and LB fractions**

47 *Electron microscopy.* Briefly, carbon-coated nickel grids were covered for 1 min with
48 corresponding fractions of interest, then washed 3 times with distilled water. They were then
49 washed again in distilled water and stained for 5 min with 2% uranyl acetate, before being air-dried.
50 Digital images were obtained with a computer linked directly to a CCD camera (Gatan) on a Hitachi
51 H-7650 electron microscope. In all cases, samples were bath-sonicated for 5 min prior to the *in*
52 *vitro* applications.

53 *Immunofluorescence analysis of noLB and LB fractions.* Indicated fractions from the sucrose
54 gradient were spread over slides coated with poly-D lysine and fixed with 4% paraformaldehyde
55 (PFA) in PBS for 30 min. Fixed slides were stained with 0.05% thioflavin S for 8 min and then
56 washed three times with 80% EtOH for 5 min, followed by two washes in PBS for 5 min. Finally,
57 all samples were washed 3 times with PBS and blocked with 2% casein and 2% normal goat serum
58 for 30 min. For immunofluorescence analyses, samples were incubated with human α -synuclein
59 specific antibody (clone syn211, Thermo Scientific, 1:1000) for 30 min, washed three times with
60 PBS, incubated with a goat anti-mouse TRITC (Jackson, 1:500), before being cover-slipped for
61 microscopic visualization using fluorescence mounting medium.

62 *Dot-blotting analysis.* To evaluate PK-resistant α -synuclein contained in noLB and LB fractions
63 derived from PD brains, each fraction was subjected to digestion with 1 μ g/ml proteinase K for 0,

64 15, 30, 45, and 60 min. The reaction was stopped by boiling for 5 min before dot-blotting with
65 syn211 antibody. To analyze their stability, noLB and LB fractions were treated with increasing
66 concentrations of urea (7 and 8M) or sodium dodecyl sulfate (SDS) (0.5, 1 and 2%) for 6 h at room
67 temperature. α -Synuclein was visualized as described above.

68 Filter retardation assay of noLB and LB fractions were probed with antibodies against,
69 phosphorylated α -synuclein (Abcam EP1536Y, 1:1000), ubiquitin (Sigma-Aldrich U5379, 1:1000),
70 p62 (Progen GR62-C, 1:1000), hyperphosphorylated tau (AT8, MN1020, ThermoFischer) or A β
71 (DAKO clone 6F/3D, 1:1000).

72 *Human α -Synuclein aggregation TR-FRET immunoassay.* Time-resolved Förster's resonance
73 energy transfer (TR-FRET)-based immunoassays were validated for total and oligomeric α -
74 synuclein (53). Ten microliters of noLB and LB samples were analyzed for total α -synuclein
75 quantification with the TR-FRET immunoassays kit against human α -synuclein aggregation kit
76 (Cisbio, #6FASYPEG) according to the manufacturer's instructions.

77 *Velocity sedimentation and density floatation α -synuclein profiles in noLB and LB fractions.* Frozen
78 noLB and LB fractions aliquots (100 μ L) were thawed and solubilized in solubilization buffer (SB)
79 to reach 10 mM Tris pH 7.5, 150 mM NaCl, 0.5 mM EDTA, 1 mM DTT, Complete EDTA-free
80 protease inhibitors (Roche), PhosSTOP phosphatase inhibitors (Roche), 1 U/ μ L Benzonase
81 (Novagen), 2 mM MgCl₂ and 2% (w/v) N-lauroyl-sarcosine (sarkosyl, Sigma) final concentrations,
82 by incubating at 37°C under constant shaking at 600 rpm (Thermomixer, Eppendorf) for 45 minutes.
83 For velocity sedimentations, a volume of 400 μ L of solubilized noLB / LB fraction was loaded on
84 top of a 11 mL continuous 5-20% iodixanol gradient (Optiprep, Sigma) in SB buffer containing
85 0.5% w/v final sarkosyl concentration, linearized directly in ultracentrifuge 11 mL tubes (Seton)
86 with a Gradient Master (Biocomp). For density floatation gradients, a volume of 400 μ L of
87 solubilized noLB / LB fraction was mixed to reach 40% iodixanol in SB buffer with 0.5% w/v final
88 sarkosyl concentration and loaded within an 11 mL 10-60% discontinuous iodixanol gradient in SB
89 buffer with 0.5% w/v final sarkosyl concentration. The gradients were centrifuged at 180,000 g for
90 3 hours (velocity) or for 17 hours (density) in a swinging-bucket SW-40 Ti rotor using an Optima
91 L-90K ultracentrifuge (Beckman Coulter). Gradients were then segregated into 16 equal fractions
92 from the top using a piston fractionator (Biocomp) and a fraction collector (Gilson). Fractions were
93 aliquoted for further analysis of their content by dot-blot. Gradient linearity was verified by
94 refractometry.

95 For dot blotting, aliquots of the collected native fractions were spotted onto Hybond PVDF 0.2 μ m
96 membranes (GE Healthcare) using a dot blot vacuum device (Whatman). For total (MJFR1) and
97 phosphorylated pS129 (EP1536Y) α -synuclein immunolabelling, a step of fixation in PBS - 0.1%

98 glutaraldehyde was performed at this point, followed by 3 washes in PBS. Membranes were then
99 blocked with 5 % (w/v) skimmed milk powder in PBS - 0.1% (v/v) Tween and probed with anti-
00 human α -synuclein (MJFR1, rabbit 1:10000, Abcam), anti-phospho pS129 α -synuclein (EP1536Y,
01 rabbit 1:5000, Abcam) or anti α -synuclein aggregate specific FILA-1 (MJFR14-6-4-2, rabbit
02 1:10000, Abcam) primary antibodies in PBS-T - 4% (w/v) BSA, and secondary goat anti rabbit IgG
03 HRP-conjugated antibodies (1:10000, Jackson Laboratories) in PBS-T 1% (w/v) milk.
04 Immunoreactivity was visualized by chemiluminescence (GE Healthcare). The amount of the
05 respective protein in each fraction was determined by the Image Studio Lite software, after
06 acquisition of chemiluminescent signals with a Chemidoc imager (Biorad). Profiles obtained by
07 immunoblot were normalized and plotted with SEM using the Prism software.

08 *FTIR microspectroscopy.* 1-2 μ L of each suspension was deposited on a CaF₂ window and dried at
09 room pressure and temperature. The protein aggregates were then measured in transmission at
10 50x50 μ m² spatial resolution with an infrared microscope (54). Depending on its size it was
11 possible to collect one to twenty spectra inside each aggregate. The infrared microscope was a
12 Thermo Scientific Continuum equipped with a MCT detector and a 32x 0.65 NA Replachromat
13 objective and matching condenser, coupled to a Thermo Scientific Nicolet 8700 spectrometer with
14 a globar source and KBr beamsplitter. The microscope was operated in dual path single aperture
15 mode. Spectra were recorded between 650-4000 cm^{-1} at 2 cm^{-1} resolution, with Happ-Genzel
16 apodization and Mertz phase correction. Spectra were processed in Omnic 9.2 for automatic
17 atmospheric correction to remove water vapor contribution.

18

19 **Rat Ventral Midbrain Primary Cultures**

20 Postnatally derived ventral midbrain cultures were prepared essentially as previously described
21 (55). Briefly, cultures were prepared in two steps. In the first step, rat astrocyte monolayers were
22 generated as follows. The entire cerebral cortex from a single rat pup (postnatal days 1–2) was
23 removed, diced, and then mechanically dissociated by gentle trituration. The isolated cells were
24 plated at 80,000 cells per well under which a laminin-coated coverslip was affixed. The cells were
25 housed at 37°C in an incubator in 5% CO₂ and were fed on glial media (89% MEM, 9.9% calf
26 serum, 0.33% glucose, 0.5 mM glutamine, and 5 μ g/mL insulin). Once confluence had been attained
27 (about 1 week in vitro), fluorodeoxyuridine (6.7 mg/mL) and uridine (16.5 mg/mL) were added to
28 prevent additional proliferation. In the second stage, which occurred 1 week later, rat pups aged
29 between 1 and 2 days were anesthetized and 1-mm³ blocks containing ventral midbrain neurons
30 were dissected from 1-mm-thick sagittal sections taken along the midline of the brain. Tissues were
31 collected immediately into cold phosphate buffer and were treated enzymatically using papain (20

32 U/mL) with kynurenate (500 μ M) at 37°C under continuous oxygenation with gentle agitation for
33 2 h. A dissociated cell suspension was achieved by gentle trituration and was then plated onto the
34 preestablished glia wells at a density of 0.5–1.7 million neurons per well. Cultures were maintained
35 in specially designed neuronal media (47% MEM, 40% DMEM, 10% Hams F-12 nutrient medium,
36 1% calf serum, 0.25% albumin, 2 mg/mL glucose, 0.4 mM glutamine, 10 μ g/mL catalase, 50 μ M
37 kynurenic acid, 10 μ M CNQX, 25 μ g/mL insulin, 100 μ g/mL transferrin, 5 μ g/mL superoxide
38 dismutase, 2.4 μ g/mL putrescine, 5.2 ng/mL Na₂SeO₃, 0.02 μ g/mL triiodothyronine, 62.5 ng/mL
39 progesterone, and 40 ng/mL cortisol) containing 27 μ M fluorodeoxyuridine and 68 μ M uridine to
40 control glial outgrowth and in 10 ng/mL glial cell derived neurotrophic factor (GDNF). They were
41 incubated for a further 7–8 days until the start of experiments. All tyrosine hydroxylase (TH)
42 neurons were counted on each plate following the addition of noLB and LB fractions after 1, 2, 5
43 and 7 days of treatment.

44

45 **Non-Human Primate Behavioral Assessment**

46 Following a 4-hour minimum habituation phase performed one day before the beginning of the
47 observations, baboon behavior was observed outside the feeding and cleaning times, in a random
48 order at two-time points (morning and afternoon), over 4 to 9 days (8 sessions per group). On the
49 1st observational time point (i.e. 1-month post-surgery), the habituation phase was performed over
50 3 days allowing the observer to recognize the animals individually. We used a scan-sampling
51 method, appropriate for time budgeting (56), in which behavioral parameters were assessed every
52 5 minutes during 2-hour sessions, resulting in 192 scans per individual. Extra observational sessions
53 were performed to avoid missing data. A unique trained observer (SC; intra-observer reliability:
54 Spearman rank order correlation R=0.987) collected the data live on the 2-time points of the study:
55 at 1- and 24-months post-surgery. The observer was standing 1 m away from the outdoor cages.
56 We focused on behavioral profiles rather than single items and used two repertoires: one reports
57 the interaction with the environment and one describes the position within the environment,
58 according to published protocols (57-59). We investigated the percentages of occurrence of each
59 item with regard to the total number of scans in order to obtain mean behavioral and postural time
60 budgets, body orientation and location profiles.

61

62 **Histopathological analysis**

63 *Extent of lesion.* To assess the integrity of the nigrostriatal pathway, tyrosine hydroxylase (TH)
64 immunohistochemistry was performed on SNpc and striatal sections. Briefly, 50 μ m free-floating
65 sections from one representative level of the striatum (anterior, medial and posterior) and serial

66 sections (1/12) corresponding to the whole SNpc were incubated with a mouse monoclonal
67 antibody raised against human TH (Millipore, MAB318, 1:5000) for one night at RT and revealed
68 by an anti-mouse peroxidase EnVision™ system (DAKO, K400311) followed by DAB
69 visualization. Free-floating SNpc sections were mounted on gelatinized slides, counterstained with
70 0.1% cresyl violet solution, dehydrated and coverslipped, while striatal sections were mounted on
71 gelatinized slides and coverslipped. The extent of the lesion in the striatum was quantified by optical
72 density (OD). Sections were scanned in an Epson expression 10000XL high resolution scanner and
73 images were used in ImageJ open source software to compare the grey level in each region of
74 interest: i.e. caudate nucleus and putamen. TH-positive SNpc cells were counted by stereology blind
75 with regard to the experimental condition using a Leica DM6000B motorized microscope coupled
76 with the Mercator software (ExploraNova, France). The substantia nigra was delineated for each
77 slide and probes for stereological counting were applied to the map obtained (size of probes was
78 100x80µm spaced by 600x400µm). Each TH-positive cell with its nucleus included in the probe
79 was counted. The optical fractionator method was finally used to estimate the total number of TH-
80 positive cells in the SNpc of each monkey hemisphere. In addition, we measured Nissl cell count,
81 the volume of SN, and the surface of TH-occupied in SN to fully characterize the pattern of
82 dopaminergic cell loss in the SN.

83 *α-synuclein pathology.* Synucleinopathy was assessed with a mouse monoclonal antibody raised
84 against human α-synuclein (syn211) and phosphorylated α-synuclein (clone11A5, Elan, 1:5000)
85 immunostaining as we previously reported (11, 30). Briefly, selected sections at two rostro-caudal
86 levels were incubated in a same well to allow direct comparison of immunostaining intensity.
87 Sections were incubated overnight at room temperature with the aforementioned antibodies. The
88 following day, revelation was performed with anti-specie peroxidase EnVision system (DAKO)
89 followed by 3,3' -diaminobenzidine (DAB) incubation. Sections were then mounted on gelatinized
90 slides, dehydrated, counterstained if necessary and coverslipped until further analysis. Grey level
91 quantification or immunostaining-positive surface quantification in forty brain regions (Fig. 2B)
92 were performed as previously described (30).

93 *Inflammation.* Inflammatory process in the striatum, in the entorhinal cortex and in the white matter
94 of noLB and LB-injected monkeys was measured through GFAP/S-100 (DAKO, Z0334/Abnova,
95 PAP11341) and Iba1 (Abcam, ab5076) immunohistochemistry. Striatal sections of all animals were
96 incubated together over night with a mix of rabbit antibodies raised against GFAP and S-100 for
97 the astroglial staining (respective dilutions 1:2000 and 1:1000) and with a goat anti-Iba1 antibody
98 for the microglial staining (dilution 1:1000). These signals were revealed with anti-specie peroxidase
99 EnVision system (DAKO) followed by DAB incubation. Sections were mounted on slides, counter-

00 stained in 0.1% cresyl violet solution, dehydrated and cover-slipped. Sections stained by GFAP-S-
01 100 were numerized at x20 magnification with a NanoZoomer (Hamamatsu, France) and the
02 quantification of GFAP-positive astrocytic reaction was estimated by a immunostaining-positive
03 surface quantification at regional levels with the Mercator software (ExploraNova, France).
04 Sections stained by Iba1 were used for the microglial morphology analysis through fractal
05 dimension quantification based on microscopic acquisitions, as previously described(60). All
06 analyses were performed blinded to the researcher.

07

08 **mRNA extraction and qRT-PCR**

09 Substantia nigra samples were homogenized in Tri-reagent (Euromedex, France) and RNA was
10 isolated using a standard chloroform/isopropanol protocol(61). RNA was processed and analyzed
11 following an adaptation of published methods(62). cDNA was synthesized from 2 µg of total RNA
12 using RevertAid Premium Reverse Transcriptase (Fermentas) and primed with oligo-dT primers
13 (Fermentas) and random primers (Fermentas). QPCR was performed using a LightCycler® 480
14 Real-Time PCR System (Roche, Meylan, France). QPCR reactions were done in duplicate for each
15 sample, using transcript-specific primers, cDNA (4 ng) and LightCycler 480 SYBR Green I Master
16 (Roche) in a final volume of 10 µl. The PCR data were exported and analyzed in an informatics
17 tool (Gene Expression Analysis Software Environment) developed at the NeuroCentre Magendie.
18 For the determination of the reference gene, the Genorm method was used(63). Relative expression
19 analysis was corrected for PCR efficiency and normalized against two reference genes. The
20 proteasome subunit, beta type, 6 (Psm6) and eukaryotic translation initiation factor 4a2 (EIF4A2)
21 genes were used as reference genes. The relative level of expression was calculated using the
22 comparative ($2^{-\Delta\Delta CT}$) method(63).

23 Primers sequences: Psm6 (NM_002798) forward: CAAGAAGGAGGGCAGGTGTACT; Psm6
24 (NM_002798) reverse: CCTCCAATGGCAAAGGACTG; EIF4a2 (NM_001967) forward:
25 TGACATGGACCAGAAGGAGAGA; EIF4a2 (NM_001967) reverse:
26 TGATCAGAACACGACTTGACCCT; SNCA (CR457058) forward: GGGCAAGAATGAA
27 GAAGGAGC; SNCA (CR457058) reverse: GCCTCATTGTCAGGATCCACA.

28

29 **Biochemical analysis**

30 *Total protein extraction and quantification.* Immunoblot analyses were performed on substantia
31 nigra, putamen and caudate nucleus. Five tissue patches were extracted on ice using 100µl of RIPA
32 buffer (50 mM Tris-HCl pH 7.4, 150 mM NaCl, 1.0% Triton X-100, 0.5% Na-deoxycholate, 0.1%
33 sodium dodecyl sulfate) with a protease inhibitor cocktail tablet (Complete Mini, Roche

34 Diagnostics). The lysate was placed on ice for 20 min and then centrifuged at 14,000rpm for 15
35 min at 4°C. The supernatant was collected and the Bicinchoninic Acid (BCA) Assay was used to
36 determine the total amount of protein in the lysates, and then stored at -80°C.

37 Based on total protein concentrations calculated from the BCA assays, aliquots of tissue lysates
38 corresponding to known amounts of total protein per lane were prepared for each animal in Laemmli
39 buffer (Tris-HCl 25mM pH=6.8, Glycerol 7.5%, SDS 1%, DTT 250mM and Bromophenol Blue
40 0.05%) for immunoblotting experiment.

41 *Biochemical fractionation.* This technique was performed as described(64). Tissue patches (n=10)
42 were homogenized in 200µl of high-salt (HS) buffer (50 mmol/L of Tris, 750 mmol/L of NaCl, 5
43 mmol/L of EDTA, and a cocktail of protease inhibitors and phosphatase inhibitors). Samples were
44 sedimented at 100,000 × g for 20 minutes, and supernatants were removed for analysis. Pellets were
45 rehomogenized in successive buffers, after which each was sedimented, and supernatant was
46 removed: HS containing 1% Triton X-100 (HS/Triton) (Variable names terminated as ultra.s1),
47 RIPA (50 mmol/L of Tris, 150 mmol/L of NaCl, 5 mmol/L of EDTA, 1% NP40, 0.5% Na
48 deoxycholate, and 0.1% SDS) (Variable names terminated as ultra.s12, and SDS/urea (8 mol/L of
49 urea, 2% SDS, 10 mmol/L of Tris; pH 7.5) (Variable names terminated as ultra.p2). Sodium dodecyl
50 sulfate sample buffer was added, and samples were heated to 100°C for 5 minutes prior to
51 immunoblot analysis.

52 *Western blot analysis.* Western blots were run in all conditions from 20µg of protein separated by
53 SDS-PAGE and transferred to nitrocellulose. Incubation of the primary antibodies was performed
54 overnight at 4°C with rabbit anti-LC3 (1:1000, Novus Biologicals), rabbit anti- LAMP-2 (1:1000,
55 Santa Cruz Biotechnology), mouse anti-TH (1:1000, Millipore), goat p62 (1:1000, Progen), mouse
56 anti human- α -synuclein (1:1000, Thermo Scientific). For detection of ubiquitinated proteins,
57 proteins were transferred on polyvinylidene fluoride membranes (Millipore) and subjected to
58 Western blot analysis using a rabbit anti-Ubiquitin (1:1000, Sigma U5379). Anti-actin (1:5000,
59 Sigma) was used to control equal loading. Appropriate secondary antibodies coupled to peroxidase
60 were revealed using a Super Signal West Pico Chemiluminescent kit (Immobilon Western,
61 Chemiluminescent HRP substrate, Millipore). Chemiluminescence images were acquired using the
62 ChemiDoc+XRS system measurement (BioRad). Signals per lane were quantified using ImageJ
63 and a ratio of signal on loading per animal was performed and used in statistical analyses.

64 *Dot-blot analysis of α -synuclein.* This technique was performed as we previously described(9, 11).
65 After heating at 100 °C for 5 min, 20 µg of protein extract was diluted in buffer (25 mM Tris-HCl,
66 200 mM Glycine, 1% SDS) and filtered through either a nitrocellulose membrane or an acetate
67 cellulose membrane (Bio-Rad, 0.2 µm pore size). Membranes were then saturated in 5% dry-

68 skimmed milk in PBS and probed with antibodies against α -synuclein (syn211, 1:1000), both α -
69 synuclein fibrils and α -synuclein oligomers (Syn-O1, 1:10000(65, 66)) (kindly provided by Prof.
70 Omar El-Agnaf). Revelation was done as described in the previous Materials and Methods section.

71

72 **Synchrotron radiation X-ray fluorescence (SR-XRF) microscopy elemental mapping of brain** 73 **tissue cryosections**

74 The synchrotron experiments were carried out at Diamond Light Source, Harwell Science and
75 Innovation Campus (Didcot, UK) with a 3 GeV energy of the storage ring and 300 mA currents
76 with top-up injection mode. All SR-XRF microscopy investigations reported herein were carried
77 out on the microfocus spectroscopy beamline (I18)(67). The micro X-ray fluorescence (μ -XRF)
78 elemental mapping were acquired at room temperature with an incident X-ray energy set to 12 keV
79 using an Si(111) monochromator and resulting in a X-ray photon flux of $2 \cdot 10^{11}$ ph/s. The substantia
80 nigra of each animal were collected from free-floating sections and mounted onto an X-ray
81 transparent metal-free 4 μ m thickness Ultralene[®] foil (SPEXCert Prep, Metuchen, NJ, U.S.A.)
82 secured to a customized Polyetheretherketone (PEEK) holder ensuring contamination-free samples
83 and reduced X-ray scattering contribution. The samples were affixed to a magnetic plate that
84 connects to the sample stage. The 4-element Si drift Vortex ME4 energy dispersive detector
85 (Hitachi Hi-Technologies Science America) with Xspress-3 processing electronics, was operated
86 in the 90° geometry, as such it minimizes the background signal. The sample-detector distance was
87 fixed (75 mm). The sample was held at 45° to the incident X-ray beam and rastered in front of the
88 beam whilst the X-ray fluorescence spectra were collected. An area of 500 μ m x 500 μ m within the
89 substantia nigra pars compacta (SNpc) was mapped for each sample with a step-size that match the
90 beam size (5 μ m) and a dwell time of 1 s per pixel due to low concentration of the element. A thin
91 (100 μ m) pellet of the NIST standards reference materials SRM1577c (bovine liver material, NIST,
92 Gaithersburg, MD, USA) was measured to calibrate experimental parameters as well as a thin-film
93 XRF reference material (AXO Dresden GmbH). This was followed by elemental quantification
94 through the open-source software PyMCA(68) in which both the reference material and the sample
95 are modelled in terms of main composition, density and thickness. The fluorescence spectrum
96 obtained from each pixel was fitted, the elemental concentration (μ g/g dry weight or ppm) maps
97 were generated and an average elemental concentration of the SNpc regions was obtained.

98

99 **Measurement of α -synuclein in monkey biological fluids samples**

00 Multi-Array 96-well plates (MesoScale Discovery, Gaithersburg, MD, USA) were coated with 30 μ l
01 3 μ l/ml MJFR1 (abcam, Cambridge, UK) as capture antibody and incubated overnight at 4°C

02 without shaking. The next day plates were washed 3 times with 150µl PBS-T [PBS (AppliChem,
03 Darmstadt, Germany) supplemented with 0,05% Tween-20 (Roth, Karlsruhe, Germany)] per well.
04 Unspecific binding of proteins was prevented by incubation with 150µl 1% BSA (SeraCare Life
05 Sciences, Milford, MA, USA)/PBS-T/well for 1 hour and shaking at 700rpm. Calibrators (kindly
06 provided by Prof. Omar El-Agnaf) were prepared from single use aliquots of α -synuclein (1µg/ml
07 stored at -80°C until use) and ranged from 25000pg/ml to 6,1pg/ml in serial fourfold dilutions. 1%
08 BSA/PBS-T served as blank. For the different specimen the following dilutions were applied: 1 in
09 10000 for whole blood and 1 in 8 for serum, plasma and CSF. All dilutions were prepared in 1%
10 BSA/PBS-T. After washing the plates 25µl calibrator solutions and diluted samples were applied
11 to the wells and incubated as indicated above. Plates were washed again and 25µl Sulfo-TAG
12 labeled Syn1 antibody (BD Biosciences, Heidelberg, Germany) diluted to 1µg/ml in 1% PBS-T
13 were applied to the wells as detection antibody. Sulfo-TAG labeling was done according to the
14 manufacturer's instruction using MSD Sulfo-TAG NHS-Ester (MSD). Incubation was for 1 hour
15 at 700rpm. Plates were washed, 150µl 2x Read Buffer (MSD) was applied and the plates were read
16 on a MSD SectorImager 2400. Data analysis was performed using WorkBench software (MSD).

19 **Neurotransmitter analysis**

20 Brain patches were dissected out on ice-cold plate, weighed and put into 1.5 ml Eppendorf tubes.
21 Samples were homogenized in methanol/water (50:50% v/v), then centrifuged at 14000 rpm for 15
22 min at 4°C(69). The supernatant was aliquoted and stored at -80°C until amino acid derivatization.
23 Glutamate and GABA content in the samples was measured by HPLC coupled with fluorometric
24 detection (FP-2020 Plus fluorimeter, Jasco, Tokyo, Japan) after precolumn derivatization with o-
25 phthaldialdehyde/mercaptoethanol (OPA) reagent(70). Thirty microliters of OPA reagent were
26 automatically added to 28 µL sample by a refrigerated autosampler kept at 4C° (Triathlon, Spark
27 Holland, Emmen, The Netherlands). Fifty microliters of the mixture were injected onto a 5-C18
28 Hypersil ODS column (3 X 100 mm; Thermo-Fisher, USA) perfused at 0.48 mL/min (Jasco PU-
29 2089 Plus Quaternary Pump; Jasco, Tokyo, Japan) with a mobile phase containing 0.1 M sodium
30 acetate, 10% methanol, 2.2% tetrahydrofuran (pH 6.5). Chromatograms were acquired and analysed
31 using a ChromNav software (Jasco, Tokyo, Japan). Under these conditions, the limits of detection
32 for glutamate and GABA were ~1 nM and ~0.5 nM, and their retention times ~3.5 min and ~18.0
33 min, respectively.

34 **Multiple-Layer Perceptrons**

36 Each Multiple-layer Perceptron (MLP) had the same architecture rule: 3 neurons as input, 3 neurons
37 in the hidden layer and 3 neurons as output. Activation function of neurons was the hyperbolic
38 tangent. Each network was trained over 1,000 presentations of a subset of the dataset. We used as
39 error measure the mean square of differences between the expected output and the actual output.
40 Our implementation comprises two parameters: a learning rate set at 0.05 (regulating the learning
41 speed), and a momentum set at 0.05 (introducing purposefully a conservatism bias). Prior to
42 learning, inputs were first scaled and centered (z scoring) in order to avoid dimensionality issues
43 and then normalized between -0.5 and 0.5. For every combination of 3 variables used as inputs, 50
44 instances of MLP were trained with different subsets of the dataset. 80% of available data has
45 been used for learning and the remaining 20% for testing the performance of the network (elements
46 of each subset were randomly (and uniformly) drawn for each network). The performance from a
47 given set of input variables was the mean of the error of the 50 instances of MLP that had data for
48 these variables as inputs. Code was written using Python and the Python scientific stack(71-73)
49 (Jones, 2001; Walt, 2011; Hunter, 2007). The code is fully available here (DOI:
50 10.5281/zenodo.1240558). Computation has been done using the Avakas cluster of the Mesocentre
51 de Calcul Intensif Aquitaine (MCIA). Rank-rank hypergeometric overlap (RRHO) test was
52 performed as previously described(74) using RRHO package (1.14.0) in R(75) on variable list after
53 ranking between experimental groups. Plotting was made using matplotlib in Python environment.
54 The association metric was based on lift calculation. Let a and b be the two variables and n_x the
55 number of combinations including variable x and n the total number of combinations considered in
56 the analysis. Lift calculation was then:

$$Lift_{ab} = \frac{n_{ab}/n_b}{n_a/n}$$

57
58 The lift calculation was then corrected for performance to avoid selection of detrimental association
59 by being divided by the mean prediction error of the duo.

60 61 **Quantification and statistical analysis**

62 Regarding the data analysis for FTIR microspectroscopy, spectra were analyzed by Principal
63 Component Analysis (PCA). PCA is a multivariate statistical analysis technique that captures
64 independent sources of variance in the data and represents them in Principal Components
65 (eigenvectors) that carry the underlying spectral information and in a Score plot that shows the
66 relation between spectra and can be used to cluster the data based on the spectral information. PCA
67 were performed in The UnscramblerX 10.3 (Camo Software) using the SVD algorithm with
68 leverage correction. Two series of preprocessing were applied prior to PCA and compared. Spectra

69 were either baseline corrected in the amide I region between 1590 and 1700 cm^{-1} and vector
70 normalized, or their second derivatives were computed and vector normalized.

71 Statistical analyses were performed with GraphPad Prism 6.0 (GraphPad Software, Inc., San Diego,
72 CA). For all experiments, comparisons among means were performed by using One-way analysis
73 of variance (ANOVA) followed, if appropriate, by a pairwise comparison between means by Tukey
74 *post-hoc* analysis. All values are expressed as the mean \pm standard error of the mean. Size effect was
75 assessed with Cohen's d analysis. In all analyses, statistical significance was set at $p < 0.05$.

76

77

78

79 **REFERENCES**

- 80 1. H. Braak *et al.*, Staging of brain pathology related to sporadic Parkinson's disease.
81 *Neurobiol. Aging* **24**, 197-211 (2003).
- 82 2. J. H. Kordower, Y. Chu, R. A. Hauser, T. B. Freeman, C. W. Olanow, Lewy body-like
83 pathology in long-term embryonic nigral transplants in Parkinson's disease. *Nat Med* **14**,
84 504-506 (2008).
- 85 3. J. Y. Li *et al.*, Lewy bodies in grafted neurons in subjects with Parkinson's disease suggest
86 host-to-graft disease propagation. *Nat Med* **14**, 501-503 (2008).
- 87 4. I. Mendez *et al.*, Dopamine neurons implanted into people with Parkinson's disease
88 survive without pathology for 14 years. *Nat Med* **14**, 507-509 (2008).
- 89 5. B. Dehay, M. Vila, E. Bezard, P. Brundin, J. H. Kordower, Alpha-synuclein propagation:
90 New insights from animal models. *Mov Disord* **31**, 161-168 (2016).
- 91 6. A. Recasens, A. Ulusoy, P. J. Kahle, D. A. Di Monte, B. Dehay, In vivo models of alpha-
92 synuclein transmission and propagation. *Cell Tissue Res*, (2017).
- 93 7. M. G. Spillantini *et al.*, Alpha-synuclein in Lewy bodies. *Nature* **388**, 839-840 (1997).
- 94 8. B. Winner *et al.*, In vivo demonstration that alpha-synuclein oligomers are toxic. *Proc*
95 *Natl Acad Sci U S A* **108**, 4194-4199 (2011).
- 96 9. M. Bourdenx *et al.*, Protein aggregation and neurodegeneration in prototypical
97 neurodegenerative diseases: Examples of amyloidopathies, tauopathies and
98 synucleinopathies. *Prog Neurobiol* **155**, 171-193 (2017).
- 99 10. N. Bengoa-Vergniory, R. F. Roberts, R. Wade-Martins, J. Alegre-Abarategui, Alpha-
00 synuclein oligomers: a new hope. *Acta Neuropathol* **134**, 819-838 (2017).
- 01 11. A. Recasens *et al.*, Lewy body extracts from Parkinson disease brains trigger alpha-
02 synuclein pathology and neurodegeneration in mice and monkeys. *Ann Neurol* **75**, 351-
03 362 (2014).
- 04 12. K. C. Luk *et al.*, Pathological alpha-synuclein transmission initiates Parkinson-like
05 neurodegeneration in nontransgenic mice. *Science* **338**, 949-953 (2012).
- 06 13. L. A. Volpicelli-Daley *et al.*, Exogenous alpha-synuclein fibrils induce Lewy body
07 pathology leading to synaptic dysfunction and neuron death. *Neuron* **72**, 57-71 (2011).
- 08 14. W. Peelaerts *et al.*, alpha-Synuclein strains cause distinct synucleinopathies after local and
09 systemic administration. *Nature* **522**, 340-344 (2015).
- 10 15. E. Bezard *et al.*, Relationship between the appearance of symptoms and the level of
11 nigrostriatal degeneration in a progressive 1-methyl-4-phenyl-1,2,3,6-tetrahydropyridine-
12 lesioned macaque model of Parkinson's disease. *J Neurosci* **21**, 6853-6861 (2001).
- 13 16. R. L. Albin, A. B. Young, J. B. Penney, The functional anatomy of basal ganglia
14 disorders. *Trends Neurosci.* **12**, 366-375 (1989).
- 15 17. G. Porras *et al.*, L-dopa-induced dyskinesia: beyond an excessive dopamine tone in the
16 striatum. *Sci Rep* **4**, 3730 (2014).
- 17 18. M. Neumann, V. Muller, H. A. Kretschmar, C. Haass, P. J. Kahle, Regional distribution
18 of proteinase K-resistant alpha-synuclein correlates with Lewy body disease stage. *J*
19 *Neuropathol Exp Neurol* **63**, 1225-1235 (2004).
- 20 19. E. Kovari *et al.*, Lewy body densities in the entorhinal and anterior cingulate cortex
21 predict cognitive deficits in Parkinson's disease. *Acta Neuropathol* **106**, 83-88 (2003).
- 22 20. L. Silveira-Moriyama *et al.*, Regional differences in the severity of Lewy body pathology
23 across the olfactory cortex. *Neurosci Lett* **453**, 77-80 (2009).
- 24 21. Y. C. Wong, D. Krainc, alpha-synuclein toxicity in neurodegeneration: mechanism and
25 therapeutic strategies. *Nat Med* **23**, 1-13 (2017).
- 26 22. B. Dehay *et al.*, Pathogenic lysosomal depletion in Parkinson's disease. *J Neurosci* **30**,
27 12535-12544 (2010).

- 28 23. C. Cook, L. Petrucelli, A critical evaluation of the ubiquitin-proteasome system in
29 Parkinson's disease. *Biochim Biophys Acta* **1792**, 664-675 (2009).
- 30 24. S. Kaushik, A. M. Cuervo, Proteostasis and aging. *Nat Med* **21**, 1406-1415 (2015).
- 31 25. E. C. Hirsch, S. Vyas, S. Hunot, Neuroinflammation in Parkinson's disease. *Parkinsonism*
32 *Relat Disord* **18 Suppl 1**, S210-212 (2012).
- 33 26. D. T. Dexter *et al.*, Alterations in the levels of iron, ferritin and other trace metals in
34 Parkinson's disease and other neurodegenerative diseases affecting the basal ganglia.
35 *Brain* **114 (Pt 4)**, 1953-1975 (1991).
- 36 27. K. Du, M. Y. Liu, X. Zhong, M. J. Wei, Decreased circulating Zinc levels in Parkinson's
37 disease: a meta-analysis study. *Sci Rep* **7**, 3902 (2017).
- 38 28. J. Y. Lee *et al.*, Cytosolic labile zinc accumulation in degenerating dopaminergic neurons
39 of mouse brain after MPTP treatment. *Brain Res* **1286**, 208-214 (2009).
- 40 29. C. T. Sheline, J. Zhu, W. Zhang, C. Shi, A. L. Cai, Mitochondrial inhibitor models of
41 Huntington's disease and Parkinson's disease induce zinc accumulation and are attenuated
42 by inhibition of zinc neurotoxicity in vitro or in vivo. *Neurodegener Dis* **11**, 49-58 (2013).
- 43 30. M. Bourdenx *et al.*, Lack of additive role of ageing in nigrostriatal neurodegeneration
44 triggered by alpha-synuclein overexpression. *Acta Neuropathol Commun* **3**, 46 (2015).
- 45 31. G. Piatetsky-Shapiro, in *Knowledge Discovery in Databases*, G. Piatetsky-Shapiro, W. J.
46 Frawley, Eds. (AAAI/MIT Press, Cambridge, MA, 1991).
- 47 32. J. P. Bolam, E. K. Pissadaki, Living on the edge with too many mouths to feed: why
48 dopamine neurons die. *Mov Disord* **27**, 1478-1483 (2012).
- 49 33. D. J. Surmeier, J. A. Obeso, G. M. Halliday, Selective neuronal vulnerability in Parkinson
50 disease. *Nat Rev Neurosci* **18**, 101-113 (2017).
- 51 34. I. Carballo-Carbajal *et al.*, Brain tyrosinase overexpression implicates age-dependent
52 neuromelanin production in Parkinson's disease pathogenesis. *Nat Commun* **10**, 973
53 (2019).
- 54 35. J. A. Rodriguez *et al.*, Structure of the toxic core of alpha-synuclein from invisible
55 crystals. *Nature* **525**, 486-490 (2015).
- 56 36. M. D. Tuttle *et al.*, Solid-state NMR structure of a pathogenic fibril of full-length human
57 alpha-synuclein. *Nat Struct Mol Biol* **23**, 409-415 (2016).
- 58 37. L. Bousset *et al.*, Structural and functional characterization of two alpha-synuclein strains.
59 *Nat Commun* **4**, 2575 (2013).
- 60 38. Y. Li *et al.*, Amyloid fibril structure of alpha-synuclein determined by cryo-electron
61 microscopy. *Cell Res*, (2018).
- 62 39. R. Guerrero-Ferreira *et al.*, Cryo-EM structure of alpha-synuclein fibrils. *Elife* **7**, (2018).
- 63 40. M. Koch, Artificial Intelligence Is Becoming Natural. *Cell* **173**, 531-533 (2018).
- 64 41. D. M. Camacho, K. M. Collins, R. K. Powers, J. C. Costello, J. J. Collins, Next-
65 Generation Machine Learning for Biological Networks. *Cell* **173**, 1581-1592 (2018).
- 66 42. T. M. Malta *et al.*, Machine Learning Identifies Stemness Features Associated with
67 Oncogenic Dedifferentiation. *Cell* **173**, 338-354 e315 (2018).
- 68 43. A. Esteva *et al.*, Dermatologist-level classification of skin cancer with deep neural
69 networks. *Nature* **542**, 115-118 (2017).
- 70 44. L. I. Kuncheva, J. J. Rodriguez, On feature selection protocols for very low-sample-size
71 data. *Pattern Recognition* **81**, 660-673 (2018).
- 72 45. D. Castelvechi, Can we open the black box of AI? *Nature* **538**, 20-23 (2016).
- 73 46. E. Diguët *et al.*, Deleterious effects of minocycline in animal models of Parkinson's
74 disease and Huntington's disease. *Eur J Neurosci* **19**, 3266-3276 (2004).
- 75 47. E. Diguët, C. E. Gross, F. Tison, E. Bezard, Rise and fall of minocycline in
76 neuroprotection: need to promote publication of negative results. *Exp Neurol* **189**, 1-4
77 (2004).

- 78 48. R. Aron Badin, M. Vadori, E. Cozzi, P. Hantraye, Translational research for Parkinsons
79 disease: The value of pre-clinical primate models. *Eur J Pharmacol* **759**, 118-126 (2015).
- 80 49. M. Ahmed *et al.*, Lentiviral overexpression of GRK6 alleviates L-dopa-induced
81 dyskinesia in experimental Parkinson's disease. *Sci Transl Med* **2**, 28ra28 (2010).
- 82 50. S. Fasano *et al.*, Inhibition of Ras-guanine nucleotide-releasing factor 1 (Ras-GRF1)
83 signaling in the striatum reverts motor symptoms associated with L-dopa-induced
84 dyskinesia. *Proc Natl Acad Sci U S A* **107**, 21824-21829 (2010).
- 85 51. G. Porras *et al.*, PSD-95 expression controls L-DOPA dyskinesia through dopamine D1
86 receptor trafficking. *J Clin Invest* **122**, 3977-3989 (2012).
- 87 52. N. M. Urs *et al.*, Targeting beta-arrestin2 in the treatment of L-DOPA-induced dyskinesia
88 in Parkinson's disease. *Proc Natl Acad Sci U S A* **112**, E2517-2526 (2015).
- 89 53. M. Bidinosti *et al.*, Novel one-step immunoassays to quantify alpha-synuclein:
90 applications for biomarker development and high-throughput screening. *J Biol Chem* **287**,
91 33691-33705 (2012).
- 92 54. G. Zandomenighi, M. R. Krebs, M. G. McCammon, M. Fandrich, FTIR reveals structural
93 differences between native beta-sheet proteins and amyloid fibrils. *Protein Sci* **13**, 3314-
94 3321 (2004).
- 95 55. W. Dauer *et al.*, Resistance of alpha -synuclein null mice to the parkinsonian neurotoxin
96 MPTP. *Proc Natl Acad Sci U S A* **99**, 14524-14529 (2002).
- 97 56. J. Altmann, Observational study of behavior: sampling methods. *Behaviour* **49**, 227-267
98 (1974).
- 99 57. S. M. Camus, C. Blois-Heulin, Q. Li, M. Hausberger, E. Bezdard, Behavioural profiles in
00 captive-bred cynomolgus macaques: towards monkey models of mental disorders? *PLoS*
01 *One* **8**, e62141 (2013).
- 02 58. S. M. Camus *et al.*, Birth origin differentially affects depressive-like behaviours: are
03 captive-born cynomolgus monkeys more vulnerable to depression than their wild-born
04 counterparts? *PLoS One* **8**, e67711 (2013).
- 05 59. S. M. Camus *et al.*, Depressive-like behavioral profiles in captive-bred single- and
06 socially-housed rhesus and cynomolgus macaques: a species comparison. *Front Behav*
07 *Neurosci* **8**, 47 (2014).
- 08 60. F. N. Soria *et al.*, Glucocerebrosidase deficiency in dopaminergic neurons induces
09 microglial activation without neurodegeneration. *Hum Mol Genet* **26**, 2603-2615 (2017).
- 10 61. P. Chomczynski, N. Sacchi, Single-step method of RNA isolation by acid guanidinium
11 thiocyanate-phenol-chloroform extraction. *Anal Biochem* **162**, 156-159 (1987).
- 12 62. S. A. Bustin *et al.*, The MIQE guidelines: minimum information for publication of
13 quantitative real-time PCR experiments. *Clin Chem* **55**, 611-622 (2009).
- 14 63. K. J. Livak, T. D. Schmittgen, Analysis of relative gene expression data using real-time
15 quantitative PCR and the 2⁻(-Delta Delta C(T)) Method. *Methods* **25**, 402-408 (2001).
- 16 64. E. A. Waxman, B. I. Giasson, Specificity and regulation of casein kinase-mediated
17 phosphorylation of alpha-synuclein. *J Neuropathol Exp Neurol* **67**, 402-416 (2008).
- 18 65. N. N. Vaikath *et al.*, Generation and characterization of novel conformation-specific
19 monoclonal antibodies for alpha-synuclein pathology. *Neurobiol Dis* **79**, 81-99 (2015).
- 20 66. M. Helwig *et al.*, Brain propagation of transduced alpha-synuclein involves non-fibrillar
21 protein species and is enhanced in alpha-synuclein null mice. *Brain* **139**, 856-870 (2016).
- 22 67. J. F. Mosselmans *et al.*, I18--the microfocuss spectroscopy beamline at the Diamond Light
23 Source. *J Synchrotron Radiat* **16**, 818-824 (2009).
- 24 68. V. A. Solé, Papillon, E., M. Cotte, P. Walter, J. Susini, A multiplatform code for the
25 analysis of energy-dispersive X-ray fluorescence spectra. *Spectrochimica Acta Part B:*
26 *Atomic Spectroscopy* **62**, 63-68 (2007).

- 27 69. D. M. de Freitas Silva, V. P. Ferraz, A. M. Ribeiro, Improved high-performance liquid
28 chromatographic method for GABA and glutamate determination in regions of the rodent
29 brain. *J Neurosci Methods* **177**, 289-293 (2009).
- 30 70. M. Marti, C. Trapella, R. Viaro, M. Morari, The nociceptin/orphanin FQ receptor
31 antagonist J-113397 and L-DOPA additively attenuate experimental parkinsonism through
32 overinhibition of the nigrothalamic pathway. *J Neurosci* **27**, 1297-1307 (2007).
- 33 71. E. Jones, E. Oliphant, P. Peterson, e. al. (2001).
- 34 72. S. van der Walt, S. C. Colbert, G. Varoquaux, The NumPy Array: A Structure for
35 Efficient Numerical Computation. *Computing in Science and Engineering* **13**, 22-30
36 (2011).
- 37 73. J. D. HUNter, Matplotlib: A 2D graphics environment. *Computing in Science and*
38 *Engineering* **9**, 90-95 (2007).
- 39 74. S. B. Plaisier, R. Taschereau, J. A. Wong, T. G. Graeber, Rank-rank hypergeometric
40 overlap: identification of statistically significant overlap between gene-expression
41 signatures. *Nucleic Acids Res* **38**, e169 (2010).
- 42 75. R. C. Team, *R: A language and environment for statistical computing*. (R Foundation for
43 Statistical Computing, Vienna, Austria, 2016).
- 44

45 **ACKNOWLEDGMENTS :** The authors wish to express their gratitude to Pr. Alan R. Crossman
46 (University of Manchester, UK) for his comments for his language supervision. We also thank Dr.
47 Marion Bosc (Cold Spring Harbor, USA) for valuable comments on the manuscript. The authors
48 thank Carmen Lagares Martínez (Head, Veterinary Service, University of Murcia) for
49 administrative assistance; Maria Fermina Ros Romero and Josefa Martínez Rabadán (University of
50 Murcia) for veterinary and husbandry support; Ana Luisa Gil, Lorena Cuenca and Ignacio
51 Mascarell from Clinical and Experimental Neuroscience group (University of Murcia) for their
52 technical help with various parts of the In Vivo part of these complex experiments. We would like
53 to thank Dr. Philippe Hantraye (MIRCCen) for providing baboon stereotactic frame. The University
54 of Bordeaux and the Centre National de la Recherche Scientifique provided infrastructural support.

55 **Funding:** This work was supported by a grant from the Michael J Fox Foundation (Project Grant
56 No. 2013-8499), Fundacion de Investigacion HM Hospitales (Madrid, Spain), the Fundación
57 Séneca (Project Grant No: FS19540/PI/14), the TARGET PD ANR grant and The Simone and Cino
58 Del Duca Prize from French Academy of Sciences. MB and MLA were supported by a Ministère
59 de l'Enseignement Supérieur et de la Recherche fellowship and the France Parkinson Foundation
60 (MB). The help of the Bordeaux Imaging Center, part of the national infrastructure France
61 BioImaging, granted by ANR-10INBS-04-0, is acknowledged. The Human α -Synuclein
62 aggregation TR-FRET immunoassay was done in the Biochemistry and Biophysics Platform of the
63 Bordeaux Neurocampus at the Bordeaux University funded by the LABEX BRAIN (ANR-10-
64 LABX-43) with the help of Y. Rufin. Computing time for this study was provided by MCIA
65 (Mesocentre de Calcul Intensif Aquitain), the public research HPC-center in Aquitaine, France. The

66 samples were obtained from the Brain Bank GIE NeuroCEB (BRIF number 0033-00011), funded
67 by the patients' associations France Alzheimer, France Parkinson, ARSEP, and “Connaître les
68 Syndromes Cérébelleux” to which we express our gratitude. The synchrotron Diamond is
69 acknowledged for provision of beam time (exp. SP13009).

70 **Author contributions:** M.B., M.V., J.O., P.D., B.D. and E.B. conceived and designed the study.
71 M.B., G.P., I.T.D., C.E., N.G.C., M.T.H., B.D. and E.B. performed surgeries. S.C. and C.E.
72 performed behavioral analysis. M.G. set up the actimetry behavioral platform. S.D., A.P. and P.A.
73 performed histologic and immunohistochemical analysis of the data. S.D., A.P. and M.L.A.
74 performed imaging experiments. E.D. performed electron microscopy analysis. F.L., M.L.A. and
75 M.L.T. performed biochemistry experiments. C.P. performed and analyzed primary cultures
76 experiment. S.B. and B.D. performed synchrotron analysis. C.S. performed infrared microscopy.
77 N.K. and B.M. performed biological fluids analysis. S.N. and M.M. performed HPLC analysis.
78 T.L.L. performed mRNA extraction and qPCR analysis. M.B., A.N., S.D., M.L.A., S.C., N.P.R.,
79 S.B., C.S., F.L., N.K., B.M., S.N., M.M., C.P., A.R., N.N.V. and O.E.A., M.T.H., P.D., M.V.,
80 J.O., B.D. and E.B. analyzed the data. M.B., A.N. and N.P.R. developed the MLP approach. M.B.,
81 M.V., J.O., B.D. and E.B. wrote the paper. B.D. and E.B. supervised the project. All authors
82 discussed the results, assisted in the preparation and contributed to the manuscript. All authors
83 approved the final version of the manuscript.

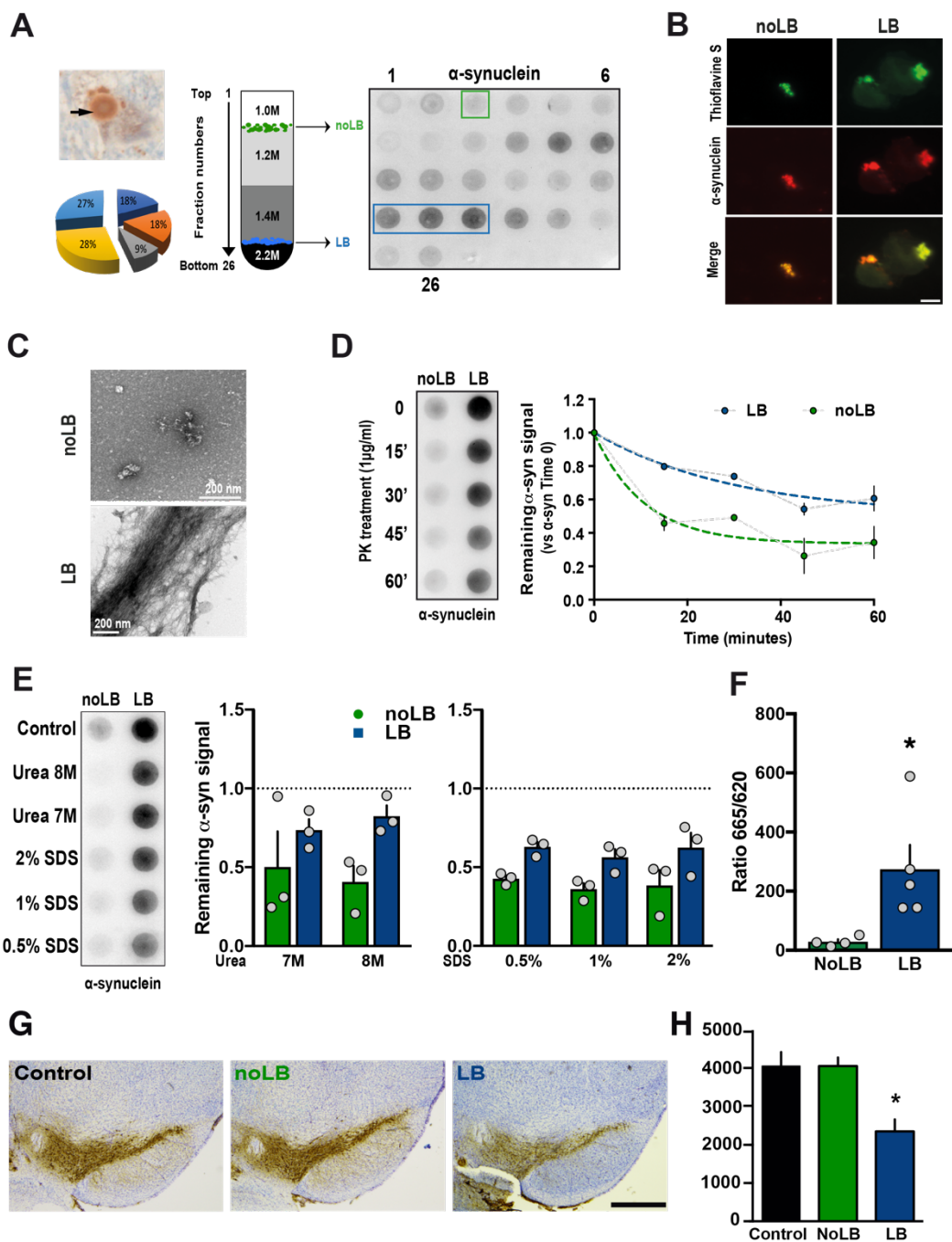
84 **Competing interests:** E. Bezard is a director and a shareholder of Motac neuroscience Ltd. All the
85 other authors have no conflict of interest to disclose.

86 **Data and materials availability:** The entire raw data set is made available to the readers (Table
87 S2). Authors chose not to provide representative examples of each procedure for the sake of space
88 and because the entire data set is fully disclosed. Further information and requests for examples
89 should be directed to and will be fulfilled by the Corresponding Contacts. Hyperlink to the machine-
90 learning code (10.5281/zenodo.1240558) is provided
91 (<https://zenodo.org/record/1240558#.XC8pqy17Su4>).

92

93

94 FIGURES

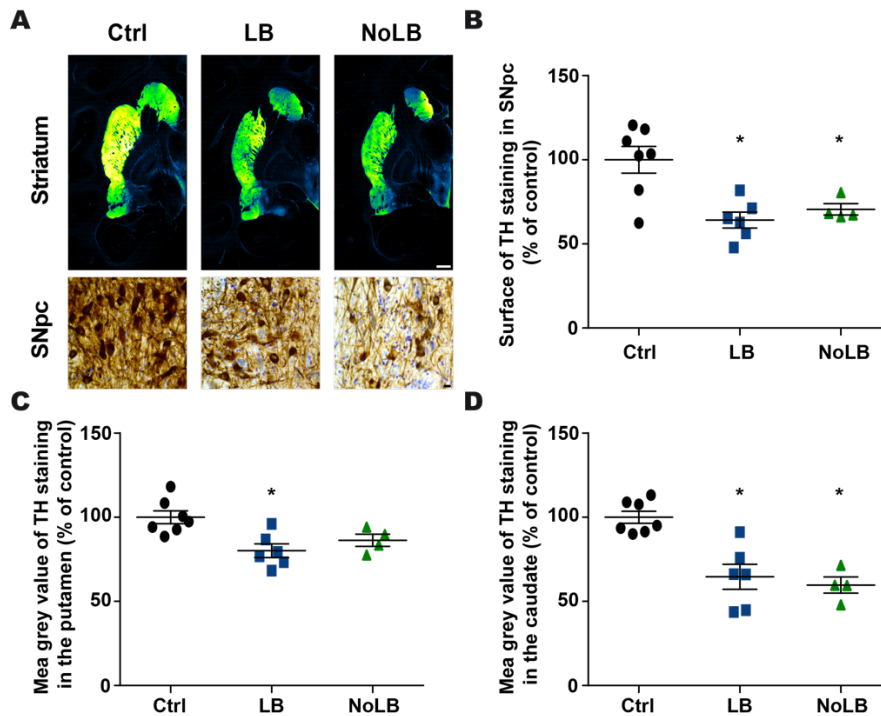


95

96

97 **Fig. 1. Purification and characterization of Lewy bodies (LB) and noLB inocula from**
 98 **Parkinson disease (PD) brains. (A, left)** Immunohistochemistry image of α -synuclein-positive
 99 LB (arrows) in nigral postmortem brain samples (PD #1; α -synuclein in brown, neuromelanin in
 00 dark-brown) before sucrose gradient purification. The pie chart indicates the relative contribution
 01 of the 5 patients to the final pool of LB and noLB inocula (**A, middle**) Schematic representation of
 02 the sucrose gradient fractionation procedure used to purify LB/noLB-containing fractions from

03 freshly frozen postmortem nigral brain tissue of 5 sporadic PD patients. **(A, right)** Filter retardation
04 assay probed with a human α -synuclein antibody to assess the presence of α -synuclein aggregates
05 in the different fractions obtained by sucrose gradient fractionation from freshly frozen postmortem
06 nigral brain tissue from sporadic PD patients (PD #1). Green rectangle indicates noLB-containing
07 fraction and blue rectangle highlights LB-containing fraction selected to prepare the mixture used
08 for injections. **(B)** Confocal examination of purified noLB and LB fractions with α -syn
09 immunofluorescence (red) and thioflavin S staining (green). Both LB and noLB present thioflavin
10 S-positive aggregates but much smaller in noLB fractions. Scale bar = 10 μ m. **(C)** Ultrastructural
11 examination of noLB and LB fractions by electron microscopy showing massive fibrils in LB
12 fractions while noLB fractions contain, besides soluble α -syn, some punctiform small size
13 aggregates. **(D)** NoLB and LB fractions derived from PD brains (left panel) were treated with 1
14 μ g/ml proteinase K for 0, 15, 30, 45 and 60 min and analyzed by immunoblotting with syn211
15 antibody. The EC50 value was determined as the concentration at which this ratio is decreased by
16 50%. The corresponding EC50 value for LB (>60 min) was approximately fourfold greater than
17 with noLB (15.23 min) **(E)** NoLB and LB fractions were treated for 6h with
18 increasing concentrations of either urea or SDS or buffer as control. Syn211 was used to detect the
19 forms of α -synuclein. The LB fractions appear to be more resistant to breakdown compared with
20 noLB fractions in both urea ($F_{(1,8)}=6.063$, $p=0.0392$) and SDS treatments ($F_{(1,12)}=17.41$, $p=0.0013$).
21 The dotted line show levels of control fractions. Comparison were made using Two-Way ANOVA.
22 **(F)** TR-FRET immunoassay analysis of noLB and LB fractions. Fluorescence measurements were
23 taken 20h after antibody. Analysis by unpaired Student's t-test ($t_{(7)}=2,623$, $p=0,0343$). *: $P<0.05$.
24 Mean \pm SEM, $n=4-5$. **(G)** Representative pictures of tyrosine hydroxylase (TH)-positive substantia
25 nigra pars compacta (SNpc) neurons (brown; Nissl staining in purple) in non-injected, noLB or LB-
26 injected mice at 4 months after injections. Scale bars=500 μ m. **(H)** Quantification of TH-positive
27 Substantia Nigra pars compacta (SNpc) neurons by stereology in control, LB- and noLB-injected
28 mice. Control mice, $n=10$, LB-injected mice at 4 months, $n=10$, No-LB-injected mice at 4 months,
29 $n=10$. One-way ANOVA followed by Tukey test for multiple comparisons. *: $p<0.05$ compared
30 with control and noLB-injected side at 4 months.

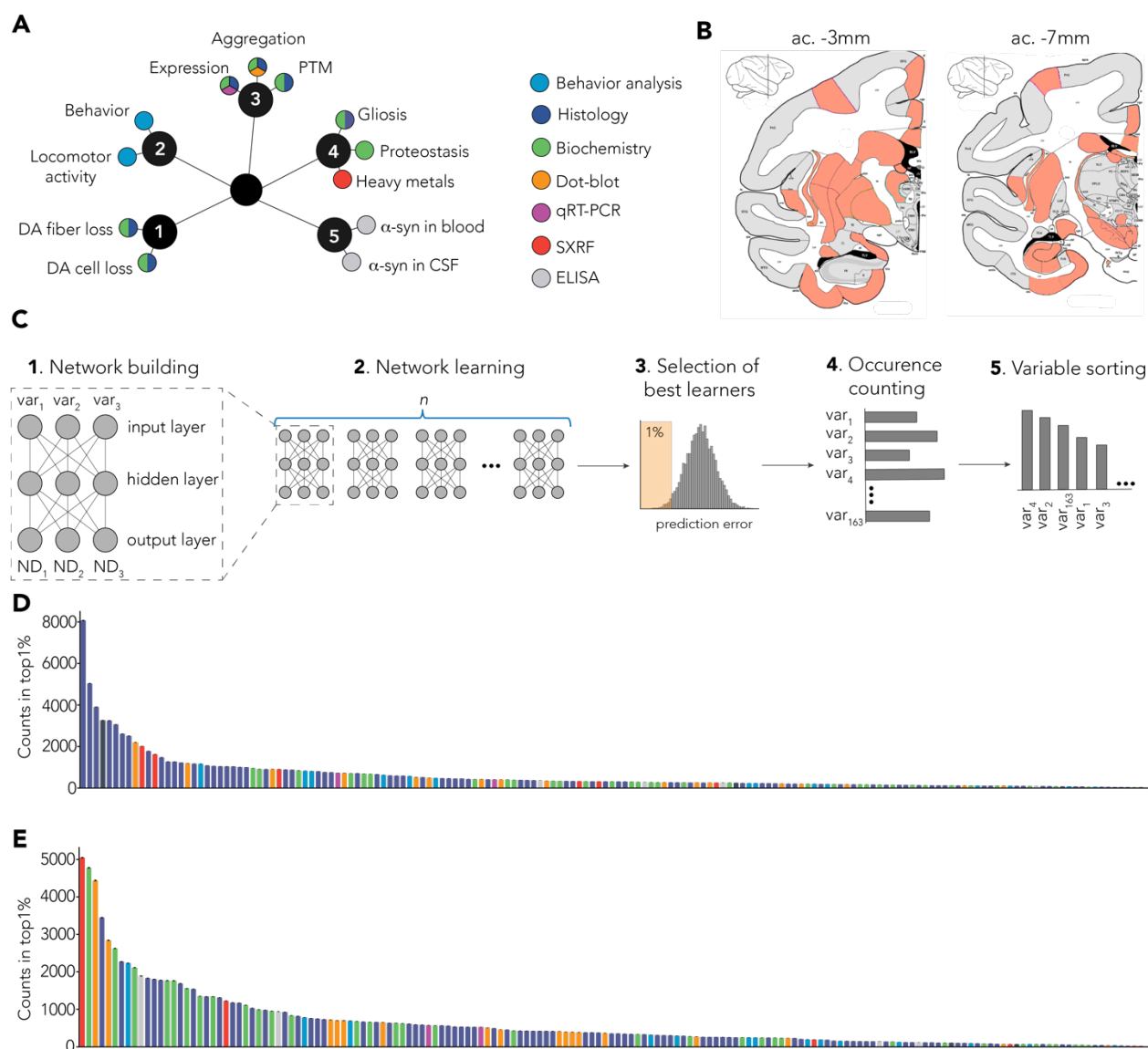


32

33

34 **Fig. 2. Intra-striatal injection of Lewy bodies (LB) and noLB fractions from Parkinson's**
 35 **disease patients induces nigrostriatal neurodegeneration in baboon monkeys.** (A) Tyrosine
 36 hydroxylase (TH) staining at striatum and Substantia Nigra pars compacta (SNpc) levels. A green
 37 fire blue LUT (lookup table) was used to enhance contrast and highlight the difference between
 38 non-injected, LB-injected and noLB-injected baboon monkeys at striatum level. Scale bars = 5mm
 39 (striatum) and 10 μ m (SNpc). (B) Scatter plot of TH immunostaining in SNpc. $F_{(2,14)}=9.439$,
 40 $p=0.0025$. Control vs LB-injected: $p=0.0029$. Control vs noLB- injected: $p=0.0248$. (C, D) Scatter
 41 plots of mean grey values of striatal TH immunoreactivity in the putamen ($F_{(2,14)}=7.313$, $p=0.0067$;
 42 Control vs LB-injected: $p=0.0059$) (C) and in the caudate ($F_{(2,14)}=16.25$, $p=0.0002$; Control vs LB-
 43 injected: $p=0.0008$; Control vs noLB- injected: $p=0.0008$) (D) in non- injected, LB-injected and
 44 noLB-injected baboon monkeys. The horizontal line indicates the average value per group \pm SEM
 45 ($n=7$ from control animals; $n=6$ for LB-injected animals; $n=4$ for noLB-injected animals).
 46 Comparison were made using One-Way ANOVA and Tukey's correction for multiple comparison.
 47 * $p < 0.05$ compared with control animals.

48

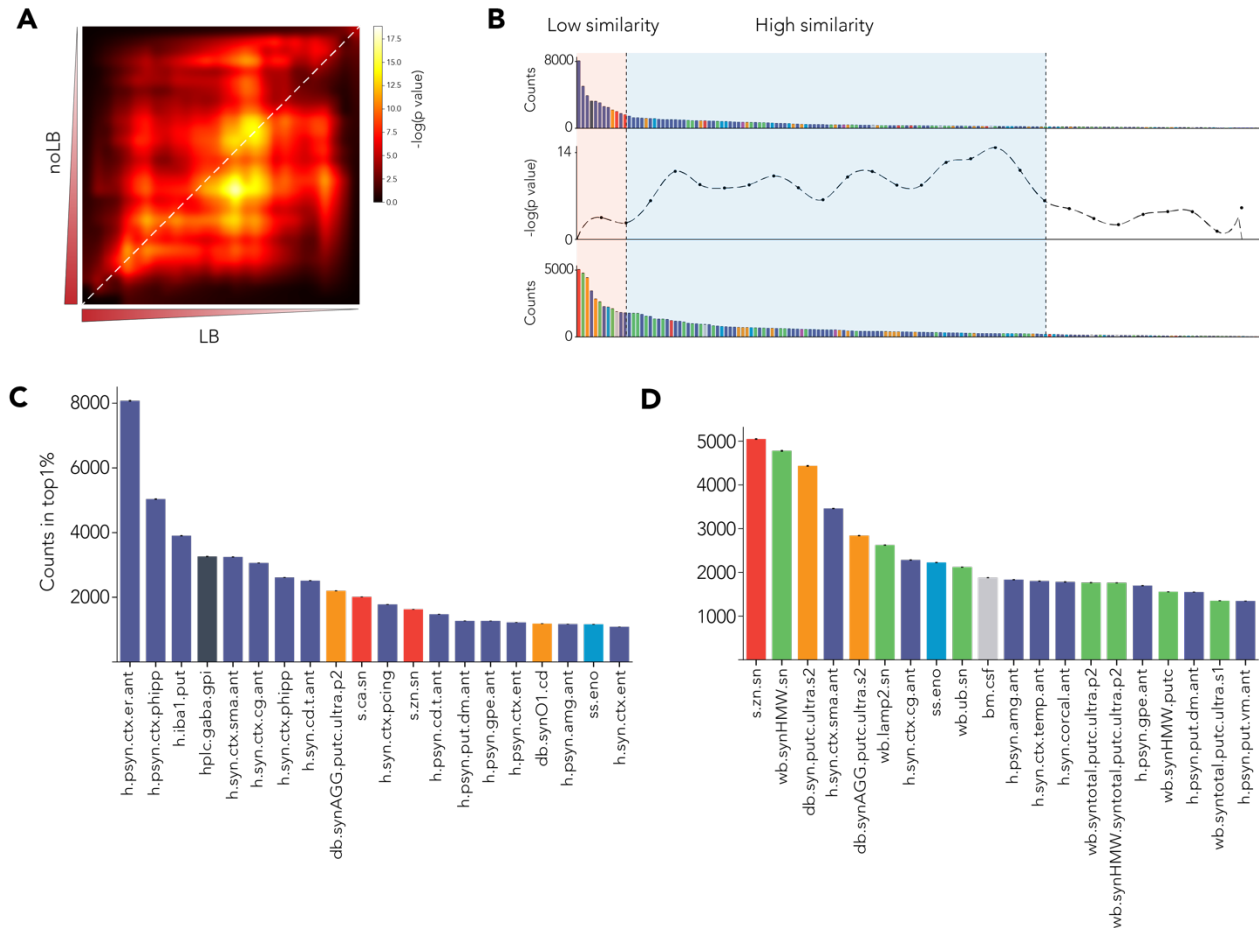


49

50

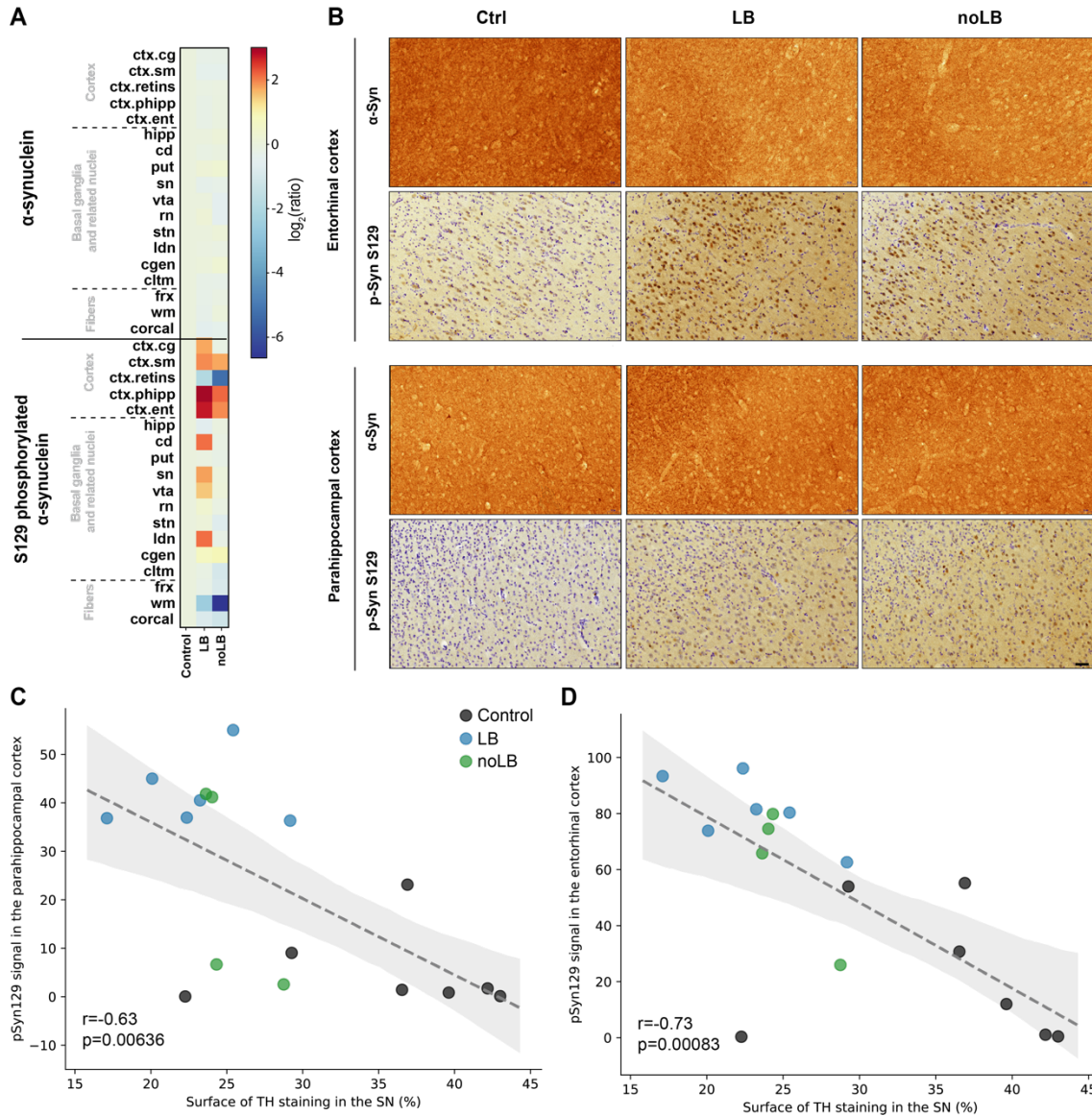
51 **Fig. 3. Multiple-layer perceptron (MLP)-based identification of specific signature.** (A) Several
 52 endpoints (n=180) were measured using multiple methods (colors). Endpoints can be grouped as
 53 clusters: 1. Dopaminergic degeneration, 2. Behavior, 3. α -syn-related pathology. 4. Non- α -syn
 54 related pathology. 5. Putative biomarkers. (B) Multiple brain regions (n=40) were investigated from
 55 coronal sections at 2 levels: anterior commissure (ac.) -3mm (striatum, entorhinal cortex) and -7mm
 56 (SNpc, hippocampus). (C) Detailed methodology. 1. Representative scheme of one MLP predicting
 57 3 neurodegeneration-related variables (ND₁, ND₂, ND₃) with 3 experimental variables as input
 58 (var₁, var₂, var₃). Out of the 180 variables measured in total, 163 were used as inputs for the MLP.
 59 2. One MLP was trained for every unique combination of 3 variables. 3. Combinations were ranked
 60 based on their prediction error and top1% were selected for further analysis. 4. Combinations were
 61 deconvoluted to extract single variables and count occurrence of individual variables. 5. Variables

62 were sorted based on the number of occurrences in the top1% of the best combination. **(D)** Raw
 63 ranking obtained for LB-injected animals. Color code highlights measurement methods as in A. **(E)**
 64 Raw ranking obtained for noLB-injected animals. Color code highlights measurement methods as
 65 in A.



68 **Fig. 4. Direct comparison of MLP-derived signatures shows specific pattern between**
 69 **experiment groups. (A)** Rank-rank hypergeometric overlap (RRHO) test between variable sorting
 70 **of LB and noLB-injected animals. Highly enriched variables are in the lower left corner. Diagonal**
 71 **(highlighted by a red dashed line) was extracted to do a bin-to-bin comparison between LB and**
 72 **noLB signatures. (B)** Signatures were aligned with RRHO and show low similarity in highly
 73 **enriched variables (light orange background) and higher similarity for lower rank variables (pale**
 74 **blue background). (C, D)** First 20 enriched variables for both LB-injected animals **(C)** and noLB-
 75 **injected animals **(D)**. Color code is similar to Fig. 2A. Detailed of variable names can be found in**
 76 **Table S1. Bars are mean +/- 99% confidence interval estimated by bootstrap.**

78
 79



81

82 **Fig. 5. Levels of α -synuclein and phosphorylated α -synuclein in different brain regions. (A)**

83 Heat map representing the surface of α -synuclein (α -syn) and S129 phosphorylated α -syn

84 immunostaining intensity in the brain of non-inoculated, LB-inoculated and noLB-inoculated

85 baboon monkeys. The heat maps show all brain regions measured and are organized according in

86 3 main groups: cortical, basal ganglia and sub-cortical areas. From top to bottom: cingulate cortex

87 (*ctx.cg*), sensorimotor cortex (*ctx.sm*), retro-insular cortex (*ctx.retins*), parahippocampal cortex

88 (*ctx.phipp*), entorhinal cortex (*ctx.ent*), hippocampus (*hipp*), caudate nucleus (*cd*), putamen (*put*),

89 substantia nigra (*sn*), ventral tegmental area (*vta*), red nucleus (*rn*), subthalamic nucleus (*stn*),

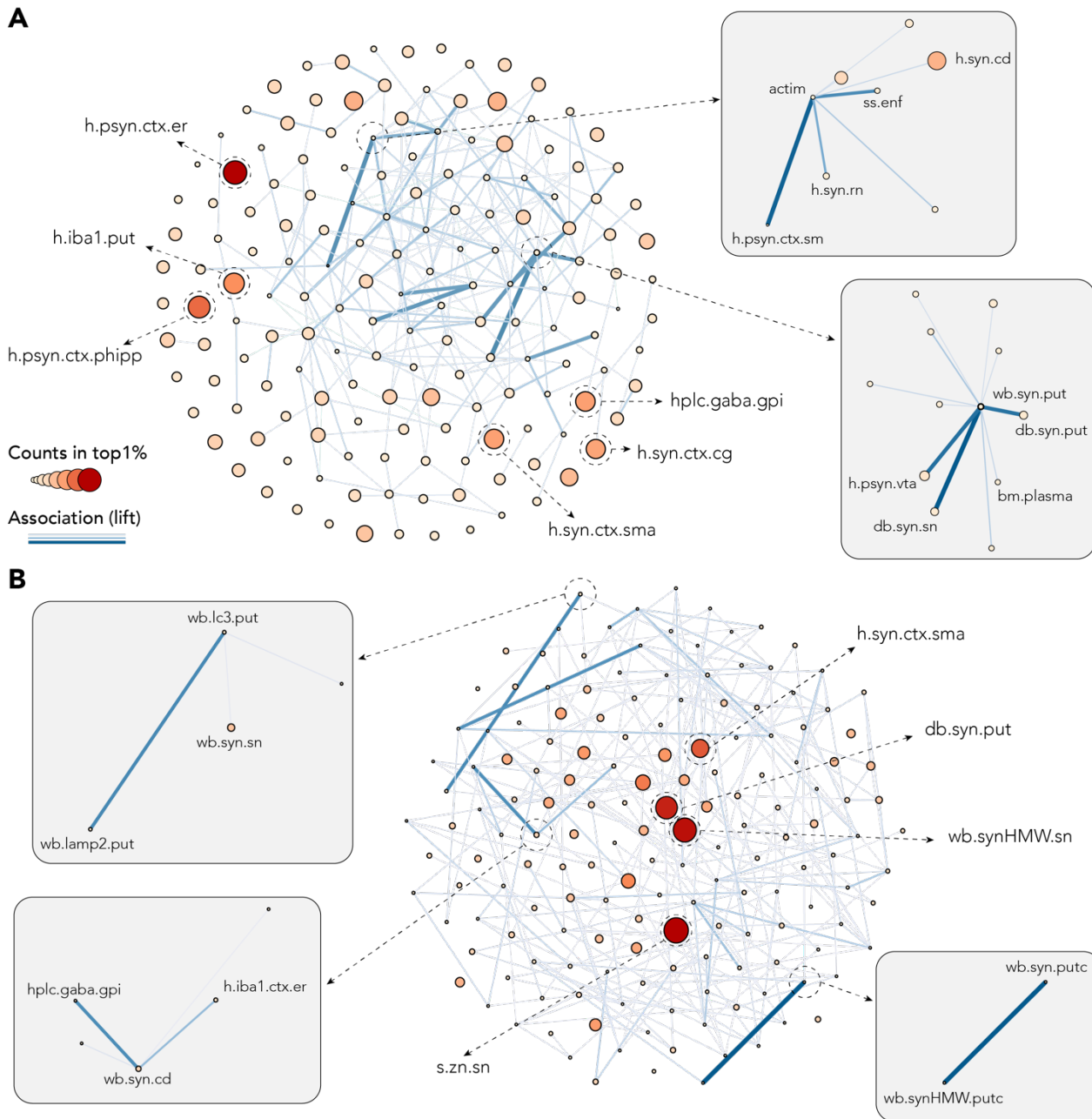
90 lateral dorsal nucleus (*ldn*), lateral geniculate nucleus (*cgen*), claustrum (*cltm*), fornix (*frx*), white

91 matter (*wm*), corpus callosum (*corcal*). The color bars represent the log₂ value of the ratio of each

92 brain regions. (B) Representative pictures of α -syn (α -syn) and phosphorylated α -syn (pSyn S129)

93 staining in the entorhinal and parahippocampal cortices. (C, D) Correlation between levels of
94 phosphorylated α -syn in the parahippocampal cortex (C) and the entorhinal cortex (D) with levels
95 of TH staining in the substantia nigra. Dotted line indicates the linear regression. Gray area indicates
96 the 95% confidence interval around of the linear regression.

97
98
99



00

01 **Fig. 6. Association metric shows independence of strong predictors and beneficial association**
02 **of weaker predictors.** Both network plots were build using number of counts in the top1% as node
03 size and color, and lift (association measure) as edges. To allow better visualization, only 10% of

04 the strongest edges are shown. **(A)** Network plot for LB-injected animals showing independence
05 of strong predictors: S129 phosphorylated α -syn (psyn) in the entorhinal (*h.psyn.ctx.er*) and the
06 para-hippocampal cortex (*h.psyn.ctx.phipp*), microglia-activation in the putamen (*h.ibal.put*), α -
07 syn in the cingulate cortex (*h.syn.ctx.cg*) and the supplementary motor area (*h.syn.ctx.sma*) and
08 GABA levels in the internal part of the globus pallidus (*hlpc.gaba.gpi*). Upper right box highlights
09 association between actimetry measure (*actim*) and a scan-sampling measure of body direction
10 toward a closed environment (*ss.enf*) with α -syn levels in the caudate nucleus (*h.syn.cd*), the red
11 nucleus (*h.syn.rn*) and psyn in the sensorimotor cortex (*h.psyn.ctx.sm*). Lower right box highlights
12 association between pathological α -syn in the putamen (*wb.syn.put* and *db.syn.put*) and the SNpc
13 (*db.syn.sn*) as well as psyn in the ventral tegmental area (*h.psyn.vta*) and peripheral levels of α -syn
14 in the plasma (*bm.plasma*). **(B)** Network plot for noLB-injected animals showing independence of
15 strong predictors: levels of Zn in the SNpc (*s.zn.sn*), pathological α -syn in the putamen (*db.syn.put*),
16 α -syn in the supplementary motor area (*h.syn.ctx.sma*) and aggregated α -syn in the SNpc
17 (*wb.synHMW.sn*). Upper left box highlights association between autophagosomes (*wb.lc3.put*) and
18 lysosomes (*wb.lamp2.put*) levels in the putamen and α -syn in the SNpc (*wb.syn.sn*). Lower left box
19 highlights association between GABA levels in the internal part of the globus pallidus
20 (*hlpc.gaba.gpi*), α -syn in the caudate nucleus (*wb.syn.cd*) and microglia activation in the entorhinal
21 cortex (*h.ibal.ctx.er*). Lower right box highlights association between soluble (*wb.syn.putc*) and
22 aggregated (*wb.synHMW.putc*) levels of α -syn in the putamen.

23

24 **Supplementary Materials:**

25 **Table S1.** List of variables used in multiple-layer perceptron analyses.

26 **Table S2.** Raw data that served for the multiple-layer perceptron analyses for all behavioral,
27 histological, biochemical, transcriptional and biophysical approaches (applied to several brain
28 areas, totalizing the quantification of 180 variables for each individual).